# Decadal Variability of Arctic Minimum Sea Ice Extent

Amélie Desmarais

Master of Science

Department of Atmospheric and Oceanic Sciences
McGill University
Montréal, Quebec, Canada

2019

A thesis submitted to McGill University in partial
fulfillment of the requirements of the degree of
a M.Sc. in Atmospheric and Oceanic Sciences

# Abstract

Uncertainty in the timing of a seasonal ice cover in the Arctic Ocean depends on uncertainty in model physics and natural variability on decadal timescales. We use the Gridded Monthly Sea Ice Extent and Concentration, 1850 Onward together with the Community Earth System Model Large Ensemble to assess whether longer term variability in the CESM is well represented, particularly in the Pacific, Eurasian and Atlantic sector of the Arctic where a longer observational record exists in an attempt to provide better estimate of the uncertainty associated with natural variability for an Atlantic, Eurasian and Pacific-centric sea ice retreat. We find that sea ice decadal (8-16 years) variability in CESM is underestimated in the Eurasian sector of the Arctic, specifically in the East-Siberian Sea, slightly overestimated in the Greenland Sea and in agreement with the observational record in the Pacific sector of the Arctic. Result also show an increased variability at interannual and decadal timescales in the transition period between a perennial and a seasonally ice-free Arctic. If the sea ice retreat continues to be Pacific-centric in the future, results from the CESM suggest that uncertainty in the timing of an ice-free Arctic associated with natural

variability may be realistic.

# Abrégé

Incertitudes dans le moment où l'Arctique deviendra saisonnièrement libre de glace dépendent d'incertitudes dans la physique des modèles et de variabilité naturelle à des échelles temporelles décennales. Nous utilisons Gridded Monthly Sea Ice Extent and Concentration, 1850 Onward et le Community Earth System Model Large Ensemble pour évaluer si la variabilité à long terme est bien représentée dans le CESM, particulièrement dans les secteurs Atlantique, Eurasien et Pacifique de l'Arctique, où des données observationnelles existent depuis plus longtemps, afin de fournir un meilleur estimé des incertitudes associées à la variabilité naturelle pour un retrait des glaces centré sur l'Atlantique, l'Eurasie et le Pacifique. Nous trouvons que la variabilité décennale (8-16 ans) de la glace de mer est sous-estimée dans le secteur Eurasien de l'Arctique, plus spécifiquement dans la mer de Sibérie orientale, est surestimée dans la mer du Groenland et est en accord avec les observations dans le secteur Pacifique de l'Arctique. Nos résultats montrent une augmentation de la variabilité à des échelles temporelles interannuelles et décennales pendant la période de transition entre un Arctique couvert de glace et un Arctique saisonnièrement libre de glace.

Si le retrait de la glace de mer continue d'être centré sur le secteur Pacifique dans le futur, les résultats du CESM suggèrent que l'incertitude dans le moment où l'Arctique deviendra saisonnièrement libre de glace associées à la variabilité naturelle seraient realiste.

# Preface

This is a manuscript-based Master's thesis and include the text of one paper. The paper will be submitted to the Journal of Climate later in summer 2019. As its introduction includes a comprehensive literature review and all the other required sections for a thesis are present, this paper satisfy all the requirement to be the actual thesis. Additional material (text and figure) are included at the end of the thesis and are not part of the paper.

## 0.1 Manuscript information

**Title**: Decadal Variability of Arctic Minimum Sea ice Extent

**Authors**: Amélie Desmarais and Bruno Tremblay

**To be submitted to**: Journal of Climate

## 0.2 Contribution of co-authors

Both Amélie Desmarais and Bruno Tremblay contributed to this research project. Amélie Desmarais realized the analysis and both co-authors contributed to the design of the project, the interpretation of the result and the writing of the paper.

# Acknowledgements

I am thankful for all the amazing experiences that I was able to live trough this degree. For making this possible, I would like to thank my supervisor Bruno. I also thank the supportive staff of the AOS department : Lucy, Amna, Manuela and Calin. I thank the sea ice research group for helping me stay motivated. But most importantly, I am thankful for the continuous support of my family and friends. We acknowledge the CESM Large Ensemble Community Project and supercomputing resources provided by NSF/CISL/Yellowstone. The Gridded Monthly Sea Ice Extent and Concentration, 1850 Onward, Version 1 was obtained from the National Snow and Ice Data Center NSIDC. I acknowledge funding from the Fonds de recherche du Québec - Nature et technologies (FRQNT). This project is a contribution to the research program of Québec-Océan and ArcTrain Canada.

# Contents

# List of Figures

# List of Tables

# 1

# Introduction

Mechanisms for long term variability in Arctic sea ice extent (SIE) are highly discussed in literature. It is known that various low frequency processes are involved. The North-Atlantic Oscillations (NAO) plays an important role in the atmospheric circulation variability as it describes the distribution of air masses between the Arctic and the subtropical Atlantic [Hurrell et al., 2003] and is related in particular to coastal ice divergence in the Eurasian sector of the Arctic. The Atlantic Meridional Overturning Circulation (AMOC) is an important factor in the Atlantic Multidecadal Variability (AMV) [Zhang et al., 2019] and is significantly correlated with SIE in various climate models [Day et al., 2012]. The strength of the AMOC however is still is underestimated across climate models [Yan et al., 2018, Kim et al., 2018]. Proshutinsky and Johnson (1997) showed the existence of two different regimes related to large scale circulation pattern in the Arctic: one that causes cyclonic circulation anomalies and one that causes anticyclonic circulation anomalies in the central Arctic [Proshutinsky and Johnson, 1997]. These two regimes are related to the location and the intensity of the Icelandic Low and the Siberian/Arctic High.

The circulation patterns also affect the surface currents in the Arctic Ocean with a period of 10-15 years [Proshutinsky and Johnson, 1997]. More quantitatively, this variability is related to the Arctic Oscillation (AO), the first Empirical Orthogonal Function (EOF) of winter Sea Level Pressure (SLP) between 20°N and 90°N and has an impact on the Transpolar drift and the Beaufort gyre [Rigor et al., 2002, Kwok et al., 2013]. The atmospheric Dipole Anomaly (DA), defined as the second EOF of winter SLP north of 70°N has been argued to be a dominant driver for record low minimum sea ice extent [Wang et al., 2009]. The DA has two centers of action within the Arctic, in both winter and summer, contrary to the AO which only has one center of action in the Arctic and two in the subpolar regions. DA is an important driver of ice export out of the Arctic as it produces strong meridional wind anomaly [Wu et al., 2006]. The Pacific Decadal Oscillation (PDO), defined as the leading EOF of monthly mean sea surface temperature (SST) anomalies over the North Pacific, affects SIE mainly in the Pacific sector and show decadal variability at a time scale of approximately 15-25 years [Mantua and Hare, 2002]. Furthermore, Pacific Ocean variability has been shown to influence the timing of a seasonally ice-free Arctic [Screen and Deser, 2019].

The Community Earth System Model version 1 (CESM1) when forced with the Representative Concentration Pathway 8.5 (RCP8.5) simulates a seasonally ice-free Arctic around 2050 [Kay et al., 2015, Jahn et al., 2016]. The trajectory of the sea ice cover is a combination of both forced (e.g: greenhouse gas emissions) and natural climate variability [Notz and Stroeve, 2018]. While we can hope to reduce the uncertainty in the timing of an ice-free Arctic (with better physics, higher resolution models and accurate forcing scenarios), there is an inherent uncertainty associated with long term (decadal to multi-decadal) climate variability. For instance, Jahn et al. (2016) have found an uncertainty of

21 years in the timing of an ice-free Arctic in the CESM Large Ensemble (CESM-LE) [Jahn et al., 2016].

Long term climate variability of SIE in the Arctic is difficult to assess from observations and validation of Global Climate Models (GCMs) at long time scales is also difficult due to the length of reliable long term pan-Arctic Observations from satellite (1979-onward; about 4 decades). There exists however long term reliable time series of SIE in the Arctic, each with different record length from long term monitoring programs in the Atlantic and Pacific sector of the Arctic from fisheries records and local economic activities and along the Eurasian coast from the [Arctic and Antarctic Research Institute, 2007]. These have been compiled into the *Gridded Monthly Sea Ice Extent and Concentration, 1850 Onward, Version 1.1*, a simple pan-Arctic dataset covering the 1850 to 2013 period [Walsh et al., 2016a]. This dataset provides an opportunity to assess the realism of longer term variability simulated by climate models for certain regions of the Arctic [Walsh et al., 2016b].

Fortuitously, the regions where longer term time series exists are colocated with regions of known source of decadal variability in sea ice extent. Variability in the Atlantic sector is mainly associated with ocean heat transport (e.g: AMOC, heat transport trough the Barents Sea Opening, [Muilwijk et al., 2018, Bitz et al., 2005]). Variability in the Eurasian sector of the Arctic is mainly associated with the atmosphere (NAO, PDO, AO) which governs variability in coastal divergence along the Eurasian coast line [Brunette et al., 2019, Williams et al., 2016, Rigor et al., 2002]. Finally, variability in the Pacific sector is associated with the ocean heat transport [Woodgate et al., 2010]. This gives hope that we can assess the realism of longer term variability in certain regions of the Arc-

tic.

Recently, a large ensemble (40) of the Community Earth System Model (CESM-LE) was produced [Kay et al., 2015]. CESM1 has a realistic representation of the Arctic (ice thickness and seasonality) [Jahn et al., 2016]. This provides a unique opportunity to assess longer term variability and quantify the uncertainty associated with natural climate variability on the timing of an ice-free Arctic. To this end, we assess the realism of the simulated longterm variability in GCMs using the historical records from the *Gridded Monthly Sea Ice Extent and Concentration, 1850 Onward, Version 1.1*.

The thesis is structured as follow: the data from observations and model is described in chapter 2, a detailed description of the statistical techniques used to analyse the variability at different frequencies is presented in chapter 3, the main findings are shown in chapter 4 and discussed in chapter 5.

# 2

# Data

## 2.1 Sea Ice Extent

We use sea ice extent data from the *Gridded Monthly Sea Ice Extent and Concentration, 1850 Onward, Version 1.1* (hereafter referred to as Sea Ice Back To 1850, SIBT1850 [Walsh et al., 2016b, Walsh et al., 2016a]). A previous study has shown that sea ice concentration in Barents and Kara seas is more realistic in SIBT1850 than in HadISST1 wang2018. The monthly sea ice concentration is given on a $0.25^\circ \times 0.25^\circ$ latitude longitude grid. We define sea ice extent as the sum of all grid cells where the sea ice concentration exceeds 15%. The sectors of the Arctic are defined on Fig 2.1. The data sources in SIBT1850 mainly includes maps of ice edge positions, information from newspapers, ship and aircraft observations, whaling ship logbook entries and digitized ice charts which are all converted to ice concentration in SIBT1850 (see Table 2.1 for an exhaustive list of the source of the observations in order of reliability and the period during which they are used). After 1978, only passive-microwave satellite observations are used. The satellite observations come

## 2.1 Sea Ice Extent

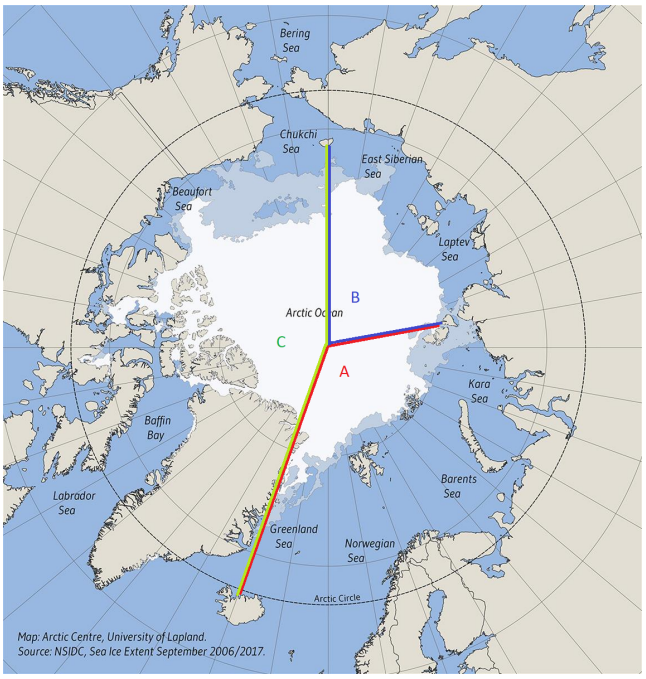


Figure 2.1: Map of the Arctic Ocean including peripheral seas and 3 regions of interest: A) the Atlantic sector, B) the Eurasian sector and C) the Pacific sector. Map: Arctic Centre, University of Lapland. Data source: NSIDC, Sea Ice Extent September 2006/2017.

from *NOAA/NSIDC Climate Data Record of Passive Microwave Sea Ice Concentration, Version 2* [Meier et al., 2013, Peng et al., 2013]. When the ice edge position was observed, a marginal sea ice zone - calculated from averaged satellite observations - was included where the sea ice concentration varies from 0 to 100%. Point observations such as whaling log book entries applies over radius of 10-20km, depending on its likelihood. The likelihood is calculated from the probability of finding sea ice in a given grid cell based on the previous and following five years.

When a sea ice observation is missing for a specific month and grid cell, the concentration is interpolated from the previous and following months (when available). If the temporal gap is longer, the ice concentration is calculated from the average of the three years

## 2.1 Sea Ice Extent

| Priority | Data Source | Period |
|---|---|---|
| 1 | Satellite observations | 1978-2013 |
| 2 | Whaling log books entries | 1850-1919 |
| 3 | Concentration fields from maps of the Danish Meteorological Institute | 1901-1956 |
| 4 | Charts from *NOAA/NSIDC The Dehn Collection of Arctic Sea Ice Charts, 1953-1986* | 1953-1986 |
| 5 | Historical ice edge position from the National Research Council of Canada | 1870-1962 |
| 6 | Digitized ice charts from the Russian Arctic and Antarctic Research Institute | 1933-1978 |
| 7 | Ice edges from the Arctic Climate System Study | 1850-1978 |
| 8 | Maps of concentration estimate from various sources forming a pan-Arctic data set [Walsh, 1978, Walsh and M. Johnson, 1979] | 1953-1978 |
| 9 | Concentration estimated from the Danish Meteorological Institute map-based edge positions from [Kelly, 1979] | 1901-1956 |
| 10 | Maps from the Naval Oceanographic Office yearbooks | 1953-1971 |
| 11 | Japan Meteorological Agency | 1968-1978 |
| 12 | Danish Meteorological Institute yearbooks, including summaries of ship report | 1901-1938 |

Table 2.1: Data source for SIBT1850 [Walsh et al., 2016a]

with the highest spatial correlation with the month with the given month. Both methods are referred to as analog filling of spatial gaps (see [Walsh et al., 2016a] for for a complete description of the analog filling method). When analog filling of spatial gaps is not possible, analog filling of spatial gaps is used instead. In this case, the ice concentration is calculated from the average of the three years with the highest spatial correlation with the nearest month where observation is available [Walsh et al., 2016b]. In general, the data coverage

is better in the peripheral seas than in the central Arctic. Analog filling of spatial gaps is often used for months prior to 1950 and analog filling of temporal gaps is mostly used for winter months (not used in the current study).

We also use SIE digitized from the book *Climate Change in Eurasian Arctic Shelf Seas* ([Frolov et al., 2009], referred to as F2009 in the following) to validate SIBT1850 in the Chukchi, East-Siberian, Laptev, Kara, Barents and Greenland seas. F2009 uses observation from different sources to infer August SIE and provides a continuous record for 1900-2003. Regular observations began in 1938 [Vize, 1940]. Airborne campaign by the Arctic and Antarctic Research Institute (AARI) since 1940 are the most reliable sources used in F2009 [Frolov et al., 2009]. F2009 also uses shipborne and airborne compilation from [Vize, 1944] for the period 1924-1939 and reconstructed ice edge positions based on observations from [Nansen, 1915] and [Lesgaft, 1913].

The length of the SIBT1850 dataset makes it particularly suitable for low frequency climate variability studies. The longest time series are for the Chukchi, Barents and Greenland seas (see Fig 2.2) where whaling ships (in the Chukchi sea) and shipping and exploration activities from the Danish Meteorological Institute (in the Greenland and Barents Seas) are abundant. In all peripheral seas, ice concentrations estimated from ice edge positions are widely used after 1901 (with the exception of 1940-1945) when observation of high order of reliability were unavailable.

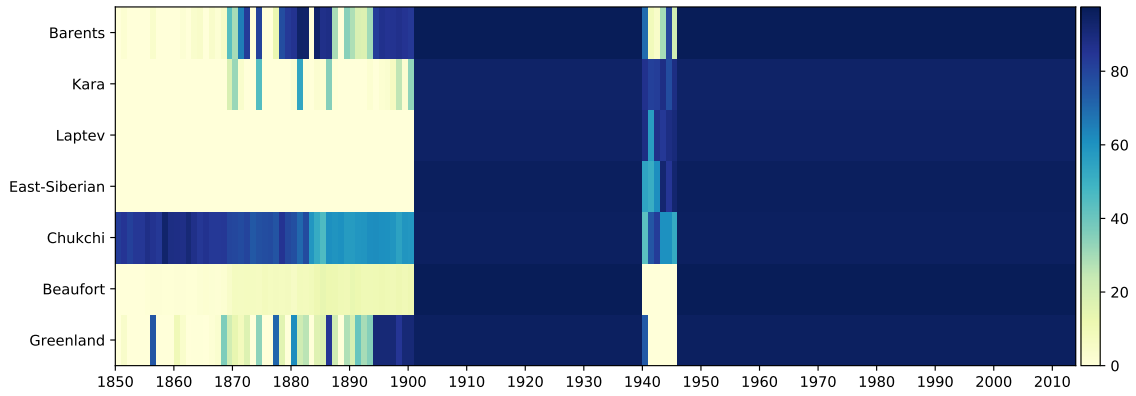


Figure 2.2: Percentage of grid cells from the Gridded Monthly Sea Ice Extent and Concentration, 1850 Onward, Version 1.1 dataset [Walsh et al., 2016b] where sea ice concentration is observed during August or September for the peripheral seas and for the Arctic.

## 2.2 Community Earth System Model-Large Ensemble (CESM-LE)

The Community Earth System Model, version 1 (CESM1) is a fully-coupled general circulation model that includes an atmosphere, ocean, land, and a sea ice component. The atmospheric component is the Community Atmospheric Model version 5.2 (CAM5.2), which includes improved parameterizations for aerosols, boundary layers and radiation compared to its predecessor CAM4 [Meehl et al., 2013]. CAM5.2 has a 1° horizontal resolution, 30 vertical levels and includes aerosol indirect effect. The land model is the Community Land Model version 4 (CLM4) which notably includes an improved representation of the snow cover and a more accurate representation of global river discharge [Lawrence et al., 2011]. The ocean model is the Parallel Ocean Program, version 2 (POP2, [Gent et al., 2011, Kay et al., 2015]). Compared to previous versions, POP2 simulates a

sharper thermocline, an improved equatorial current structure and reduced sea surface temperature and salinity biases in the North Atlantic [Danabasoglu et al., 2012]. POP2 however underestimates the multidecadal variability of the Atlantic Meridional Overturning Circulation (AMOC) when compared to observations, possibly due to a weak low frequency variability of the North Atlantic Oscillations (NAO, [Kim et al., 2018]). The sea ice component is the Community Ice CodE version 4 (CICE4), a recent version of the Los Alamos Sea Ice Model [C. Hunke and Lipscomb, 2008]. The thermodynamic component takes into account brine pocket dynamics [Bitz and Lipscomb, 1999] and the dynamic component is based on the Elasto-Viscous-Plastic (EVP) rheology [Hunke and Dukowicz, 2002]. POP2 and CICE4 have a $1^{\circ}$ resolution and uses a curvilinear coordinate system with the North Pole located over Greenland to avoid the singularities at the North Pole.

The CESM-Large Ensemble (CESM-LE) includes 40 ensemble members for the 1920-2100 period. A preindustrial control run with constant forcing is integrated to quasi equilibrum for a few centuries. Ensemble Member (EM) 1 is initialized from January 1, year 402 of the control run simulation. The model uses historical forcing for 1920-2005 and follows the representative concentration pathway 8.5 (RCP8.5) for the 2006-2100 period [Meinshausen et al., 2011]. EM-2 is initialized from January 1st 1920 of EM-1 with ocean temperatures lagged by one day. EM 3-40 are initialized with atmospheric temperature from EM 1 with round-off level perturbations [Kay et al., 2015]. At the end of the $21^{st}$ century, all the ensemble members have reach a global warming of approximately 5 K and the Arctic is ice-free in all ensemble members. The large number of ensemble members, the forcing scenario and the length of the simulations make this model suitable for studying low frequency internal climate variability and climate change

## 2.2 Community Earth System Model-Large Ensemble (CESM-LE)

[Kay et al., 2015, Jahn et al., 2016].

# 3

# Method

We use wavelet analysis to study the dominant modes of variability of September sea ice extent in each of the Arctic peripheral sea and how they evolve in time. The Continuous Wavelet Transform (CWT) of a discrete sequence $x_n$ is defined as [Torrence and Compo, 1998]:

$$W_n(s) = \sum_{n=0}^{N-1} x_n \psi^* \left[ \frac{(n' - n)\delta t}{s} \right] \tag{3.1}$$

where $\psi$ is a conjugated, scaled and translated wavelet. The initial wavelet can have different shapes but must have zero mean and be localized in time and frequency space. In the following, we use the Morlet wavelet, a plane wave modulated by a Gaussian. This wavelet allows both good temporal and spectral resolution. Other wavelets used in the field include Paul and derivative of a Gaussian (for a review see [Torrence and Compo, 1998]). We first compute the wavelet power by translating the wavelet through the signal and changing its scale. For a Morlet wavelet, the scale is equal to 0.97 times the period of a sinusoidal

function [Torrence and Compo, 1998]).

In the following, the CWT is computed over normalized sea ice extent anomalies time series. The anomaly time series are constructed by removing the ensemble mean (or linear detrending for observations) and dividing by the mean standard deviation of all ensemble members. We use two distinct periods for detrending the observations to be able to capture the recent decrease in sea ice extent. The periods are usually separated in the 1990's, the exact year being chosen to minimize the $\chi^2$. We quantify the significance and reliability of the CWT using the cone of influence (COI). In a CWT, the time series is padded with zeros at the beginning and end to bring its total length to the next power of 2. The zeros are removed afterward, but the discontinuities remain. The COI corresponds to the region of the spectrum where the impact of the discontinuity at the edges are considered important. The wavelet power from the edge is considered negligible if it has dropped by a factor of $e^{-2}$ (based on [Torrence and Compo, 1998]). The part of the wavelet spectrum in the COI must be ignored. The significance of the results are assessed using the 95% confidence levels from a red-noise spectrum, meaning that the null-hypothesis is assumed to be a mean power spectrum corresponding to a lag-1 autocorrelation [Gilman et al., 1963]. Results are considered significant for time period outside the COI and if the frequency identified in the time series is significant at the 95% level.

We also examine the variations of power over a range of scales using the scale-averaged wavelet power. It corresponds to the weighted sum of the wavelet spectrum for scales within a specific interval (in the following decadal or scales corresponding to the 8-16 years band). We then obtain the evolution in time of the variability for a certain frequency range. This method is relevant in our study since it allows for the comparison of many time series in

one plot precisely for decadal variability.

We can also compute maps of wavelet power of a time series for a specific band to obtain a spatial visualization of decadal variability. For each grid cell, we compute the CWT of the sea ice concentration anomaly, select a specific scale range of the wavelet spectrum and compute a value for the average wavelet power. For the maps, power is not in log to allow the localisation of hot spots of variability more easily.

# 4

# Results

## 4.1 Validation of the SIBT1850

The SIBT1850 is a well documented pan-Arctic dataset with long term temporal coverage ideal for low frequency variability study. We use F2009 - a dataset with broad coverage, both temporally and spatially, particularly in the Eurasian Artic - to validate SIBT1850 for the period 1900-2003 in two specific regions: the Greenland, Barents and Kara seas (GBK) and the Laptev, East-Siberian and Chukchi seas (LEC). For this comparison, we use the peripheral sea definition of F2009. SIBT1850 is well correlated with F2009 for the 1900-2003 period in both GBK and LEC (R=0.72 and R=0.74 respectively). Overall, the August SIE and inter-annual variability in SIBT1850 in the GBK and LEC seas are in good agreement with F2009 (see Fig 4.1). When the analog filling method is not used (i.e: when only observations are used), the interannual variability is weak before 1900. The analog filling method in SIBT1850 offers a significant improvement in the retrieval of sea ice extent variability (see Fig 4.1, for the 1850-1900 time period).

## 4.1 Validation of the SIBT1850

In the GBK region, SIE from SIBT1850 and F2009 and their variability generally agree (see Fig 4.1a). The 10-year running standard deviation from SIBT1850 and F2009 are in agreement. There are two periods where SIBT1850 and F2009 differ. For the 1910-1925 time period, SIE from SIBT1850 is in average $0.35 \times 10^6 \text{km}^2$ higher than F2009. The use of different information to compute SIE in the two data set may explain this bias. For example, SIBT1850 mostly uses observations from the Danish meteorological institute for this time period while F2009 does not. For the 1950-1965 time period, SIE from SIBT1850 is in average $0.38 \times 10^6 \text{km}^2$ higher than F2009. A new data source in SIBT1850 - the pan-Arctic dataset from [Walsh and M. Johnson, 1979] - starts in 1953 and is used in the Greenland, Barents and Kara seas among others.

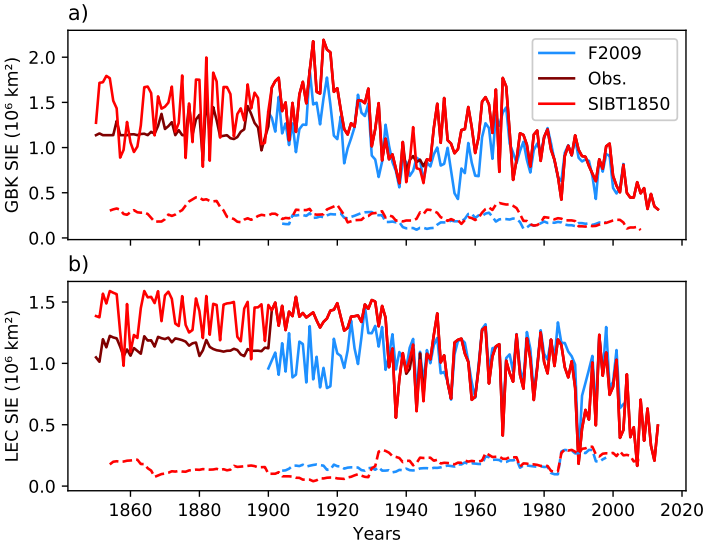


Figure 4.1: August SIE from SIBT1850 and F2009 (solid lines) and their 10-years running standard deviation (dashed lines) for the a) Greenland, Barents and Kara seas (GBK) and b) Laptev, East-Siberian and Chukchi seas (LEC). The line identified as Obs. is the SIBT1850 ice extent where absent data are padded with average available data instead of using the analog filling method.

In the LEC region, SIE from SIBT1850 and F2009 and their variability agree very well for 1940-2013. The inter-annual variability is significantly smaller in SIBT1850 than in F2009 for the 1900-1930 time period as can be seen from the 10-years running standard deviation 2.6 times smaller. Interannual variability in F2009 for the 1900-1930 period resembles the interannual variability of the following decades and is similar to the variability for 1850-1900 in SIBT1850, giving hints that interannual variability in F2009 could be more realistic in 1900-1930 than in SIBT1850. Whaling ship records were more seldom in the Chukchi sea after 1900 and SIBT1850 relies more heavily on the analog filling method leading lower variability. From 1930-1940, SIBT1850 SIE in the LEC seas features an abrupt loss of approximately 0.46 million $km^2$ in SIE. This period coincides with the inclusion of ice charts from the Russian Arctic and Antarctic Research Institute and maps from the Danish Meteorological Institute. Spatial maps of ice concentration from SIBT1850 show that this decrease is mainly due to a important sea ice retreat in the Laptev sea and partly in the East-Siberian sea (see Fig 4.2). This retreat could be linked to a change in wind pattern, as they highly influence sea ice [Rigor et al., 2002] and are an important factor for sea ice variability in this area [Brunette et al., 2019, Zhang et al., 2018]. Ice in the Kara and Chukchi seas is also changing between 1924 and 1945

## 4.2 Variability in the CESM-LE and SIBT1850

### 4.2.1 Inter-annual Variability

The min SIE significantly decreases over the time series both across the Arctic and in the three regions of interest (see Fig 4.3 and 4.4). In the Arctic Ocean, the sea ice starts to decrease in extent around 1990 (see Fig 4.3a). The observations of SIE anomaly mostly fit

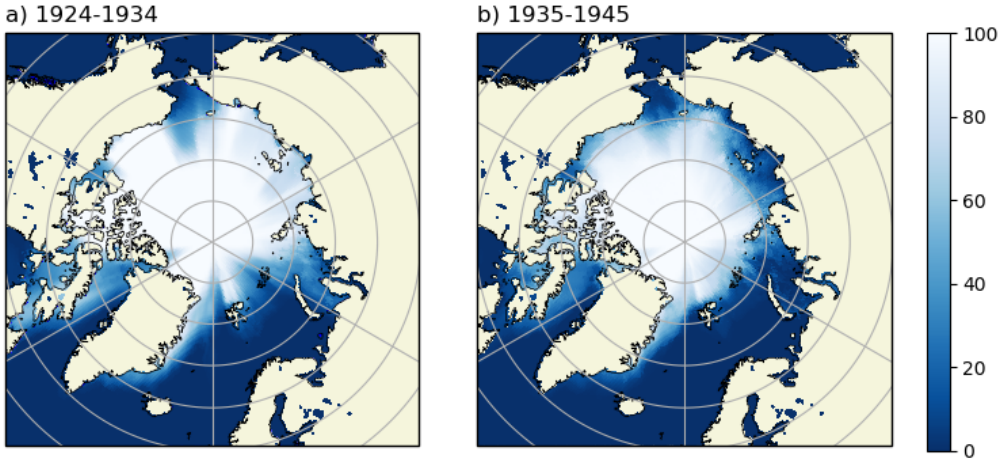


Figure 4.2: Mean August sea ice concentration from SIBT1850 for a)1924-1934 and b) 1935-1945.

in the $3\sigma$ range (99% likelihood). The observed min SIE mostly lies within the envelope of simulated min SIE, except for the two record low min SIE in 2007 and 2012. The min SIE anomalies lies mainly within the 3 standard deviation from the CESM-LE except for 6 anomalous years trough the time series. In the transition period to a seasonally ice-free Arctic, the inter-annual variability increases in the simulated min SIE anomalies. This is in accord with the 20th and 21st century simulations of the Community Climate System Model, version 3 [M. Holland et al., 2008]. Contrary to Holland et al. (2008), distribution of positive and negative anomalies about the ensemble mean are not symmetrical, with negative anomalies more localized in time over a 30-year period in the early part of the decline and positive anomalies lasting from 2010-2060 for 60 years (see Fig 4.3b). This is due to the reduced sea ice extent after 2030 which decreases the likeliness of an important negative anomaly. We refer to the period between 2010 and 2040 as the transition period from perennial to seasonal sea ice characterized by enhanced inter-annual variability of

the CESM-LE and variability across EMs. In the observational record, we see a hint of increased inter-annual variability starting in the 1990's (see Fig 4.3c), but nothing that was not observed before. For instance, large positive anomalies in the running standard deviation were observed in the 1950's and 1960's.

Regionally, the interannual variability is largest in the Atlantic sector, followed by the Pacific sector and the Eurasian sector (see Fig 4.4). In the Atlantic sector, the inter-annual variability is large with a spread of ensemble members representing approximately 30% of the total SIE (see Fig 4.4a). In the Atlantic sector, the ice extent is influenced by ocean heat transport [Bitz et al., 2005] an local winds. Most of the Atlantic sector is not covered by sea ice during summer which limits the variability drastically. The inter-annual variability in the $20^{th}$ century is such that we only see a small increase in the SIE anomalies in both positive and negative anomalies in during the transition period to a seasonally ice-free Arctic. SIE from SIBT1850 mostly falls within the range of the CESM-LE and its variance is significantly lower than the CESM ensemble mean, including for the recent decades exept in 1950-1960.

In the Eurasian sector, the min sea ice extent starts to decrease around 2000. The decrease is the fastest of all 3 sectors, and the variability is enhanced (see Fig 4.4b). Indeed, the deviation from the ensemble mean increases from 2000 to 2040, and the 20-year running standard deviation doubles in the CESM-LE during the transition period to a seasonally ice-free Arctic. The observed SIE anomaly falls within the range of the model, and the retreat is similar to the ensemble memeber with the fastest decline in CESM-LE. The variance is similar for the model and the observations and a significant increase in the observed variance occurs in 1980 - in accord with the CESM-LE - and has remained until now.

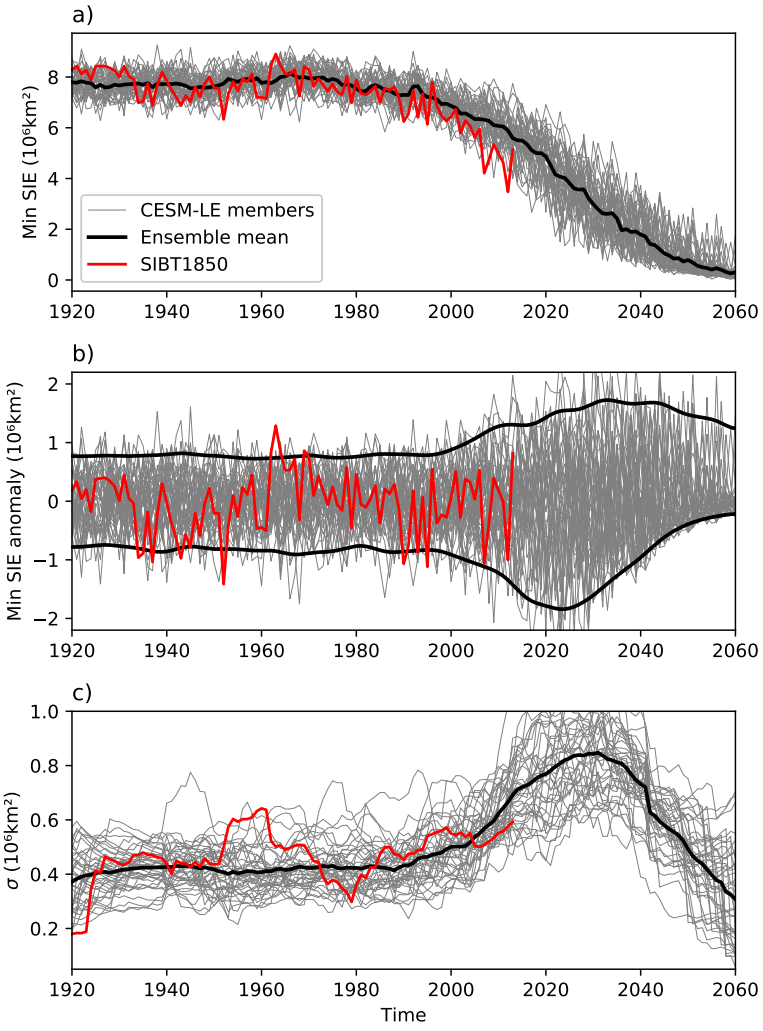


Figure 4.3: a) Arctic minimum SIE from the the 40 ensemble members of the CESM-LE (grey), the ensemble mean (black) and from SIBT1850 (red). b) Minimum SIE anomaly from the 40 ensemble members of the CESM-LE (grey), 3$\sigma$ (black) for positive and negative anomalies and SIBT1850 (red). c) 20-years running standard deviation from the 40 ensemble members of the CESM-LE (grey), ensemble mean (black) and SIBT1850 (red). Figure based on Holland et al. (2008)

In the Pacific sector, the decrease in sea ice extent is slower and also occurs later (see Fig 4.4c). The interannual variability is relatively small when compared with the total area

of the sector (anomaly represents 20% of the SIE, see Fig 4.4c and f). The increase in the variance of the CESM-LE also occurs later in the time series than in the other regions, in agreement with a later decrese in SIE. The variance of the SIBT1850 is steadily increasing since 1930 with a sudden increase the recent years.

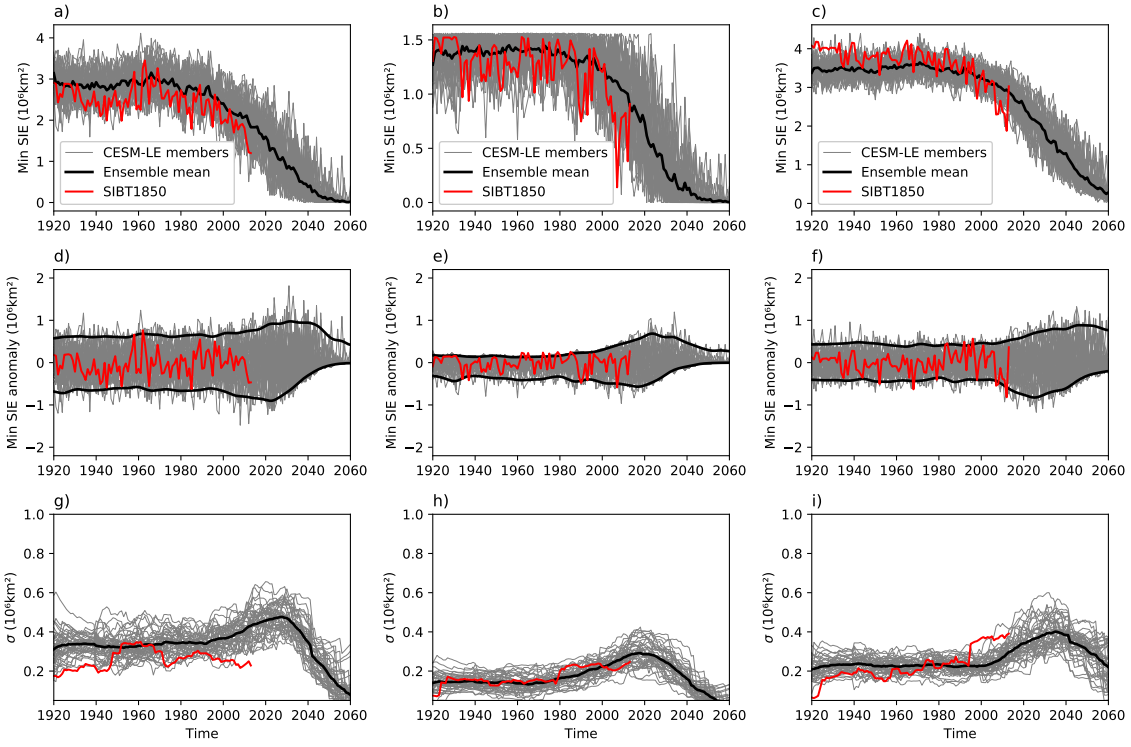


Figure 4.4: a, b, c) Minimum SIE from the the 40 ensemble members of the CESM-LE (grey), the ensemble mean (black) and the observation from SIBT1850 (red). d, e, f) minimum SIE anomaly from the 40 ensemble members of the CESM-LE (grey), $3\sigma$ (black) for positive and negative anomalies and SIBT1850 (red). g, h, i) 20-years running standard deviation from the 40 ensemble members of the CESM-LE (grey), ensemble mean (black) and SIBT1850 (red). Left column is for the Atlantic sector, middle column is for the Eurasian sector and right column is for the Pacific sector. Figure based on [M. Holland et al., 2008].

In summary, the variability increases during the period of transition between the 20$^{th}$ century and the seasonally ice-free state in the mid 21$^{st}$ century. This is mainly the case

when we look at the entire Arctic Ocean and in the Eurasian sector. In the observations, the variability starts to increase in the 80's in the Arctic, in the Eurasian sector, and in the Pacific sector following the model. The sudden increase in variability observed in the Eurasian sector of the Arctic in 1980 coincides with the beginning of satellite era, which may cause this rise in inter-annual variability.

### 4.2.2 Decadal Variability

#### Wavelet Power Spectra

In the following, we present results on the decadal variability of the simulated (CESM-LE) and observed (SIBT1850) minimum sea ice extent anomalies using wavelet analysis. In particular, we present wavelet power spectra of the min SIE anomaly for EM-28 of the CESM-LE (see Fig 4.5a). This ensemble member is representative of most of the ensemble members. The wavelet power spectrum shows significant high frequency variability for most years and significant low frequency variability at the 8-16 years timescale between 2000 and 2040 when the variability is significant at the 95% confidence level. We also observe variability at the 20-30 years scale for most EMs, but this variability is generally not significant at the 95% confidence level in part due to edge effects. Multi decadal variability is present sporadically at all times with higher power at the end of the time series while decadal variability shows a significant increase after 2000. Decadal and inter-annual variability weaken at the very end of the time series because of the lack of sea ice.

The most common pattern across ensemble members is a significant increase in inter-annual, decadal and multi-decadal variability around 2020 followed by a decrease at the end of the time series. The multidecadal signal is generally not significant and is also outside

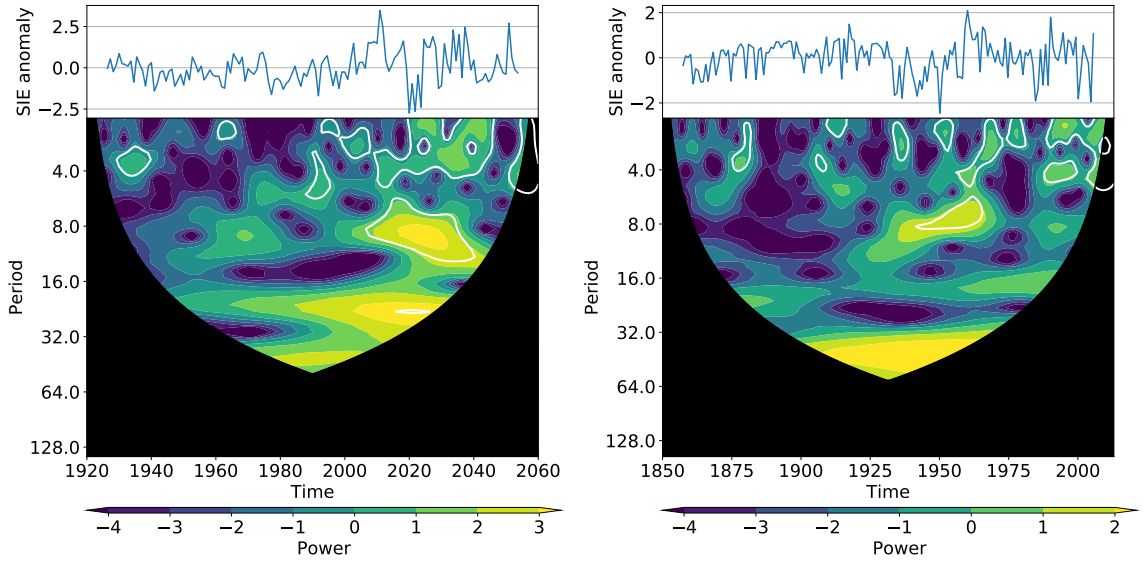


(a) EM-28 (b) SIBT1850

Figure 4.5: Normalized minimum SIE anomaly in the Arctic Ocean (top) and its wavelet power spectrum (bottom) for a) EM-28 of CESM-LE and b) SIBT1850. The vertical axis is the period which is related to the scale of the wavelet transform. The horizontal axis is the time, from 1920 to 2060. The white line is the 95% confidence level. The shaded region is the COI (i.e. the region influenced by edge effects). Light colors mean high power and good correlation with a sinusoidal signal of the corresponding period, dark colors mean low power and weak correlation with a sinusoidal signal of the corresponding period. Powers are in log.

the COI only for a short period at the middle of the time-series. In fact, we can average the spectrum obtained from all EMs and find a cone of high power at all frequencies centered around 2030, with the multidecadal signal being more spread earlier in time (not shown). The center of this local maximum is co-located with the peak in the ensemble mean 20-years running standard deviation (from Fig 4.3). This implies that the increase in decadal and multidecadal variability coincides with the increase in inter-annual variability during the transition period. In principle, increase in low frequency variability (40-50 years) could be used as an early signal for transition to a seasonal ice cover. The low-frequency signal

is however difficult to recognize as edge effects are important and the 95% confidence level is still difficult to obtain. A spread in the signal at multidecadal timescales could also be related to a longer decorrelation time for low frequencies [Torrence and Compo, 1998]. Overall, most of the ensemble members show a pattern of variability similar or weaker than the observations over the Arctic (see Fig 4.5b).

In the Atlantic sector, most of the ensemble members of CESM-LE show higher decadal variability and similar multidecadal variability than SIBT1850 (see Fig 4.6a and 4.6b). After 1930, variability in the SIBT1850 increases due to better data coverage an more accurate representation of the ice cover, but remains lower than most of the CESM-LE ensemble members even during satellite era (see Fig 4.6b). Seven of the 40 ensemble members have a similar or slightly weaker pattern of variability at decadal to multidecadal timescales than the SIBT1850 during their overlapping period (1920-2013, see Fig 4.6b). These seven ensemble members that are in line with the variability of the 1920-2013 period project an increased variability centered in 2030.

In the Eurasian sector, SIBT1850 poorly captures any sort of variability in minimum SIE until 1950 with nearly zero interannual variability in the earlier part of the record (see Fig 4.6d). This low variability is related to weak coverage in the sector. Wavelet spectra from the CESM EMs are quite different from one another before 2000 but generally in agreement with SIBT1850 (result not shown). 90% of the CESM EMs present an important signal at decadal to multidecadal variability around 2030. In SIBT1850, 15-20-years oscillations are present from 1950 to 1990 generally below the 95% significance level, with higher power in the recent decades (see Fig 4.6d). This timescale is the same as that of the Arctic Ocean Oscillation (AOO), which has a 14-16 years signature

[Proshutinsky et al., 2015].

In the Pacific sector, the CESM-LE shows weak decadal variability in agreement with SIBT1850 for 1920-2013. SIBT1850 features an insignificant but persistent signal across the time series at multidecadal timescales (30-40-years) that is not captured by most of the ensemble CESM-LE members. CESM-LE predicts an increase in decadal to multidecadal variability in 2040, which is 10 years later than in the other regions (see Fig 4.5e). The Pacific sector includes the Canadian Arctic Archipelago and the waters north of Greenland, where we expect thick and persistent sea ice for a longer time than in the other Arctic regions, which may explain the late increase in variability.

## 4.2 Variability in the CESM-LE and SIBT1850

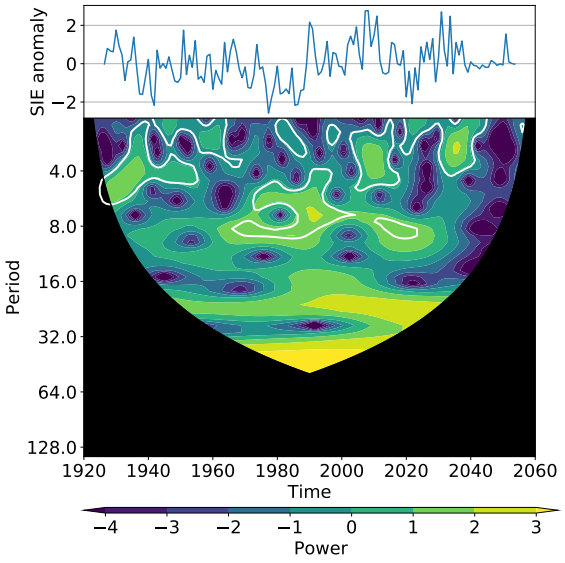


(a) EM-28 Atl.

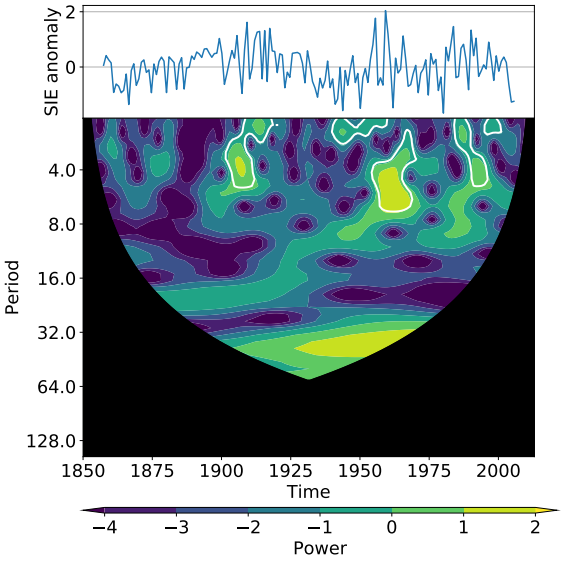


(b) SIBT1850 Atl.

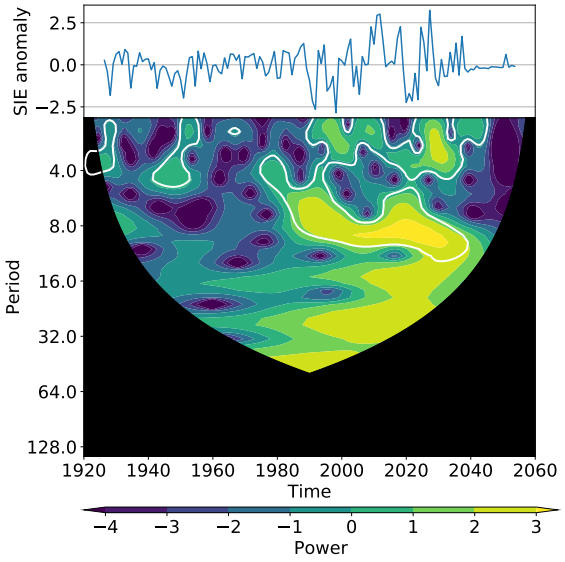


(c) EM-28 Eur.

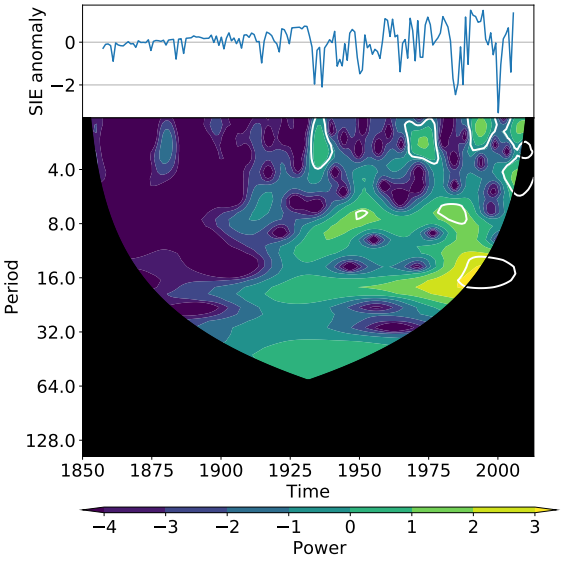


(d) SIBT1850 Eur.

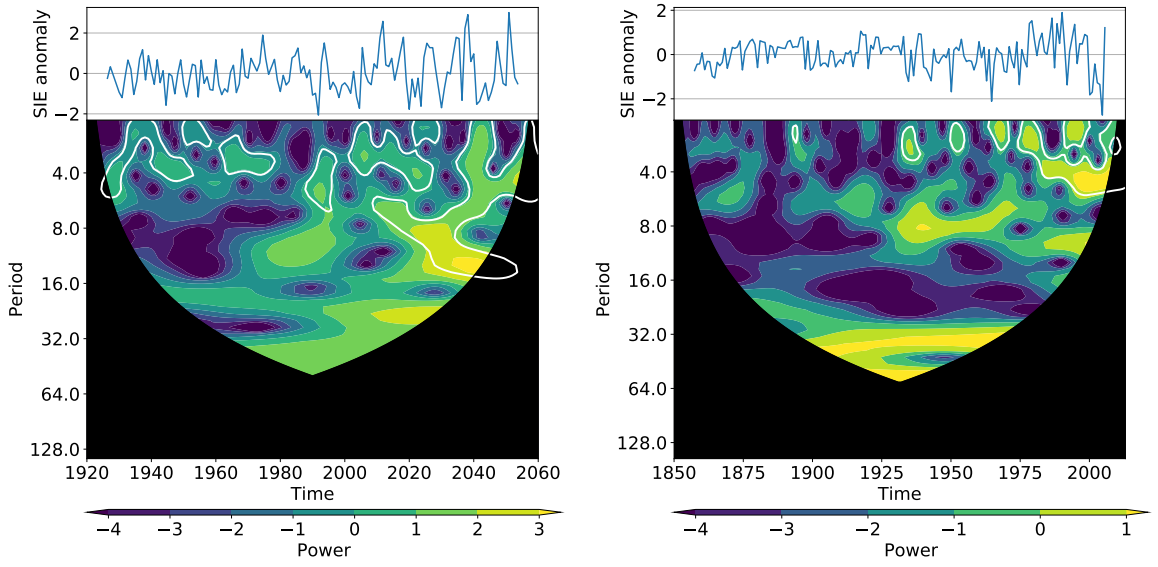


(e) EM-28 Pac.

(f) SIBT1850 Pac.

Figure 4.5: Normalized minimum SIE anomaly (top) and its wavelet power spectrum (bottom) for a) EM-28 of CESM-LE and b) SIBT1850 in the Atlantic sector, c) EM-28 of CESM-LE and d) SIBT1850 in the Eurasian sector, e) EM-28 of CESM-LE and f) SIBT1850 in the Pacific sector. The vertical axis is the period which is related to the scale of the wavelet transform. The horizontal axis is the time, from 1920 to 2060. The white line is the 95% confidence level. The shaded region is the COI (i.e. the region influenced by edge effects). Light colors mean high power and good correlation with a sinusoidal signal of the corresponding period, dark colors mean low power and weak correlation with a sinusoidal signal of the corresponding period. Powers are in log.

### Scale-averaged Wavelet Power

The scale-averaged wavelet power of the 40 ensemble members for CESM-LE and SIBT1850 allows for a direct comparison of the simulated variability with the observa-

tions. At the 8-16 years timescale, the observed variability in SIBT1850 is within the range of the CESM scale-averaged wavelet power across the Arctic, although most ensemble members generally underestimates 8-16 years variability particularly for the 1930-1960 period (see Fig 4.6). The SIBT1850 variability is not significant at the 95% level (it is significant at the 90% level for 1935-1945) but most of the CESM-LE ensemble members are not. Decadal variability then decreases and stay relatively low in SIBT1850. Decadal variability in CESM-LE also stays relatively low except during the transition period 2010-2060. The uncertainty in the timing of a seasonally ice-free Arctic mainly stems from this high power at decadal timescales. The observations however still show no sign of increased variability at decadal time scale. Note that the scale-averaged wavelet of SIBT1850 for the last 10 years of the time series are affected by edge effects.

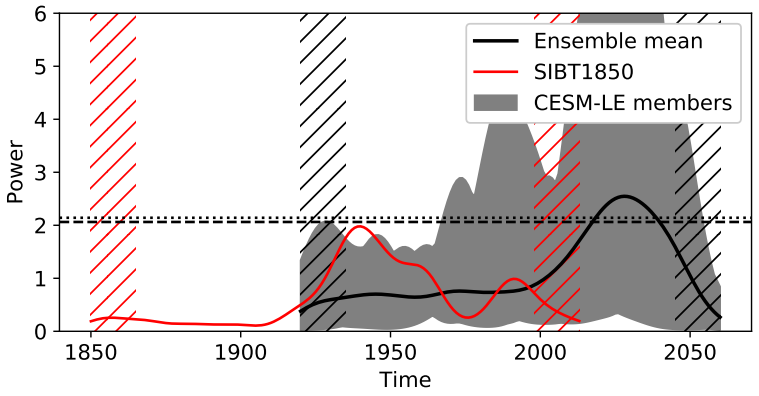


Figure 4.6: Scale-averaged wavelet power over the 8-16 years band for minimum SIE anomalies for CESM-LE ensemble member range (grey), ensemble mean (black) and SIBT1850 (red). The dotted black line is the the 95% confidence level for the model and the dashed black line is the the the 95% confidence level for the observations. The hatched regions are inside the COI and have to be ignored.

### 4.2 Variability in the CESM-LE and SIBT1850

Regionally, we observe that decadal variability in SIBT1850 lies within the range of the CESM over most of the time series and in all sectors except in the late 20th century in the Eurasian and Pacific sectors where it is significantly underestimated (see Fig 4.7). In the Atlantic sector, SIBT1850 decadal variability is lower than CESM-LE and lies within the range of the CESM for all times. Mechanisms responsible for decadal variability in this region (e.g: surface Atlantic waters, ocean heat transport, AMOC) cause an overestimates decadal variability in SIE in the model. In the Eurasian sector of the Arctic, decadal variability in the CESM-LE is about half the one of SIBT1850 for the last 30 years (see Fig 4.7b). The model predicts an increase in variability centered around 2015 while the observations show an important increase centered in 1995. It is a possibility that the CESM-LE is "late" compared to SIBT1850 in representing this increase in decadal variability (about 20 years later). This is in line with the fact that GCMs tend to underestimate the rate of decline of sea ice in the Arctic [Melia et al., 2016]. Finally, decadal variability in the Pacific sector from CESM-LE is comparable to the one from SIBT1850 with an earlier sign of increased natural variability at decadal timescales as for the Eurasian sector.

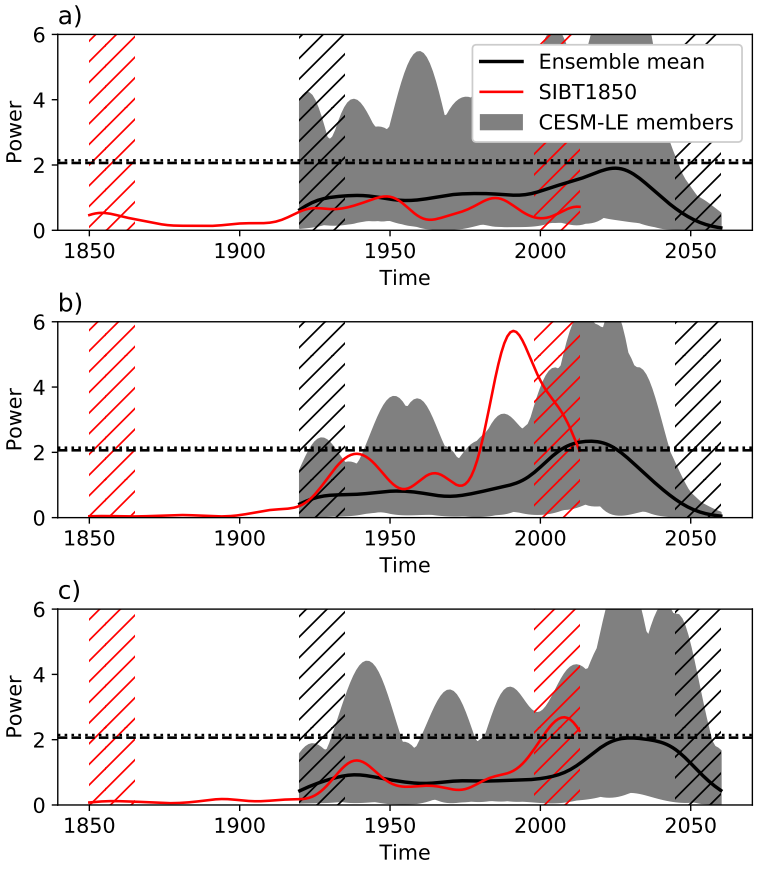


Figure 4.7: Scale-averaged wavelet power over the 8-16 years band for minimum SIE anomaly for CESM-LE ensemble member range (grey), ensemble mean (black) and SIBT1850 (red) for the the a) Atlantic, b) Eurasian and c) Pacific sector of the Arctic. The dotted black line is the the 95% confidence level for the model and the dashed black line is the the the 95% confidence level for the observations. The hatched regions are inside the COI and have to be ignored.

## 4.2 Variability in the CESM-LE and SIBT1850

### Regional Analysis

The wavelet power map from CESM-LE and SIBT1850 (see Fig 4.8) includes sea ice concentration for 1930-2013 because the availability of observations in SIBT1850 prior to 1930 is not sufficient and because the variability is unrealistically low. In facts, sub-sampling the September sea ice concentration from the satellite era, so that the coverage is the same as SIBT1850 for the 1880-1910 period, only allow the detection of decadal variability in the Greenland, Chukchi and Barents seas. These patterns of decadal variability are unrealistically weak and do not correspond to the result when including the full coverage. When using the later time period (1930-2013), the spatial patterns are the same when the satellite record is sub-sampled. Varying the spatial resolution of the grid cells from SIBT1850 gives a coarser resolution for Fig 4.8b but does not change the pattern not the intensity of decadal variability. The wavelet power maps show that the 8-16 years variability is located in the Marginal Ice Zone (MIZ, defined here as the zone between 15% and 80% ice concentration). The CESM-LE grid cells with high wavelet power are mostly close to the 15% concentration limit, in agreement with SIBT1850.

In the Atlantic sector, decadal variability for the period 1930-2013 is generally greater in the CESM-LE than in SIBT1850, especially in the Greenland sea. In fact, none of the 40 EM accurately represent decadal variability in the Greenland sea (see Fig 4.9) REVOIR. In the Eurasian sector, the model shows weaker decadal variability particularly in the East Siberian sea when compared with the observations. A dozen of the CESM-LE ensemble members (ensemble members 1, 2, 9, 14, 16, 29, 35, 37 and 39) show a similar pattern than SIBT1850 in the map of wavelet power for the 8-16 years band over the East-Siberian and Laptev seas. Nonetheless, the intensity remains slightly lower

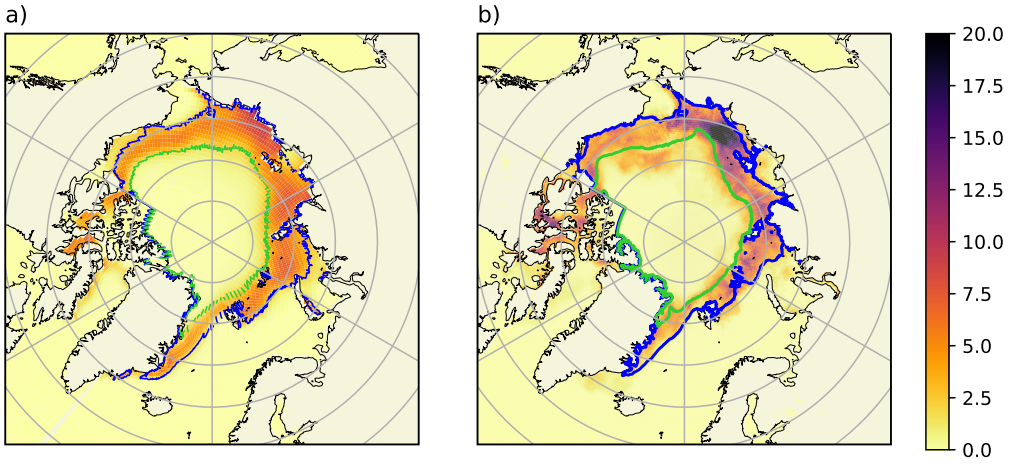


Figure 4.8: Map of wavelet power over the 8-16 years band for minimum sea ice concentration from a) CESM-LE ensemble mean and b) SIBT1850 for the period 1930-2013. The green contours are the average 80% ice cover and the blue contours are the average 15% ice cover. Darker color indicates greater 8-16 years variability.

in every ensemble member. In the Pacific sector, decadal variability in generally weaker in the CESM-LE than in the SIBT1850, although some ensemble members show similar magnitude as in SIBT1850. Decadal variability in the observations is important north of Bering Strait, suggesting and oceanic process in cause. Some ensemble members also show decadal variability north of Bering Strait as in the observations. Ocean heat fluxes trough the Bering Strait influences sea ice and has been increasing in the last decades [Woodgate et al., 2010, Woodgate et al., 2012]. Furthermore, decadal timescale variability is observed in the Pacific [Mantua and Hare, 2002]. The observed sea ice decadal variability might be linked to possible inaccurate representation the PDO and the Bering strait inflow, which are important factors for an accurate representation of the changing SIE in the Arctic [Screen and Deser, 2019].

## 4.2 Variability in the CESM-LE and SIBT1850

A map of wavelet power for the satellite era shows an increase of variability in the observations (not shown). During this period (1980-2013), only 4 CESM-LE ensemble members (ensemble members 14, 16, 32 and 35) feature a similar pattern in the East-Siberian and Laptev seas than SIBT1850, which has a larger magnitude than for the 1930-2013 period. The intensity remains lower in the CESM-LE and, of the 4 EM in agreement with SIBT1850, none also accurately represents the variability in the Greenland and Barents seas, which is enhanced compared to the 1930-2013 period. The sea ice extent from recent decades show a clear rise in decadal variability in tha Atlantic sector of the Arctic. Some ensemble members feature larger decadal variability than SIBT1850 but none of the particular ensemble members present a similar spatial pattern. Notably, decadal variability in the Eurasian sector of the Arctic is sometimes displaced to the west, or variability is too strong in the Pacific sector of the Arctic. The 1980-2013 period only includes 2 to 3 cycles of 8-16 years. This is a short time series to study decadal variability in the Arctic. Indeed, edge effects affect half of this time series, but the observed increases of decadal variability in the wavelet power map are consistent with the one observed in the wavelet power spectrum outside of the COI.

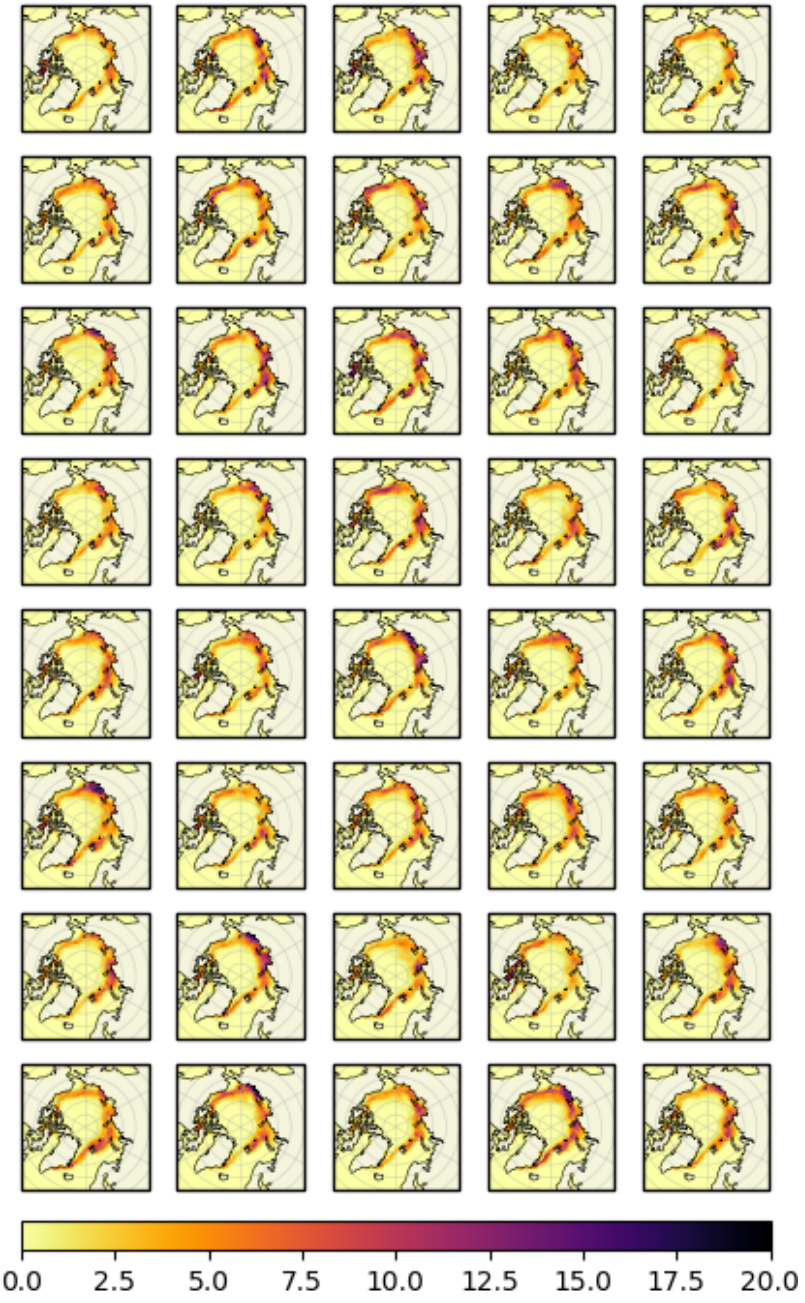


Figure 4.9: Map of wavelet power over the 8-16 years band for minimum sea ice concentration from all CESM-LE ensemble members for the period 1930-2013. The green contours are the average 80% ice cover and the blue contours are the average 15% ice cover. Darker color indicates greater 8-16 years variability.

# 5

# Discussion

## 5.1 Atlantic Sector

The wavelet analysis has shown that decadal variability in CESM-LE is overestimated in the Greenland sea, a region influenced by Atlantic waters. Over the last decades, the strength of the AMOC has a 7-9 years cycle [Mercier et al., 2015]. On the other hand, Kim et al. (2018) showed that the AMOC is underestimated in the CESM-LE [Kim et al., 2018]. Therefore, the strength of the AMOC is not directly the cause, but other ocean-related processes might be involved. Other studies have observed large decadal variations (5-10 year period) in the ocean heat transport and more precisely in the Atlantic sector of the Arctic [Muilwijk et al., 2018]. Ocean Heat Transport (OHT) is concurrent with sea ice area change in the Barents sea and also been linked to rapid decease in sea ice extent in the CESM-LE and other GCMs [Årthun et al., 2012, Auclair and Tremblay, 2018, Holland et al., 2006]. The overestimation of decadal variability in the Greenland sea in this model could be related to an unrealistic representation of the ocean heat transport in the Atlantic sector.

A comparison of OHT from the Fram Strait, Barents Sea Opening (BSO) and Bering Strait show a good agreement between the CESM-LE and observations through the BSO and an underestimation of OHT through the Bering and Fram Straits in the CESM-LE [Auclair and Tremblay, 2018]. We find that sea ice decadal variability is well represented in the CESM-LE in the Barents sea, in agreement with the good representation of OHT. Decadal variability in the Greenland sea is overestimated in the CESM-LE south of the Fram Strait, meaning that this variability can be linked to other oceanic current recirculating in this area, such as the Norwegian Atlantic Current [Orvik and Skagseth, 2003]. Analysis of sea surface temperature also show a 8-12 years variability in the Atlantic [Delworth et al., 2013], which could be linked to sea ice. The ocean heat transport in the Atlantic sector has been linked with the Arctic Oscillations (AO) [Årthun and Schrum, 2010] which show cycles corresponding to the observed decadal variability. Furthermore, the North Atlantic Oscillations (NAO) can influence the storm activity in the Atlantic sector of the Arctic [Hurrell et al., 2003] and greatly influence sea ice conditions [Simpkins, 2018].

## 5.2 Eurasian Sector

The wavelet analysis has shown that 8-16 years variability in CESM-LE is underestimated the East-Siberian sea. This is timescale is in accordance with a surface current corresponding to a prevailing Arctic High atmospheric pressure and its 10-14 years oscillation period [Proshutinsky and Johnson, 1997]. This regime would correspond to predominant northward surface currents over the region of interest, moving ice away form the coastline. Furthermore, Itkin and Krumpen (2017) demonstrated how winter dynamics influence anomalies of summer sea ice extent and thickness [Itkin and Krumpen, 2017]. Since winter winds are usually northward along the Eurasian coastline [Dewdney, 1979], we can expect

coastal polynyas to form and low ice concentration to last trough the the following summer. Williams et al. (2016) showed that late-winter sea ice drift anomaly away from the coastline is strongly correlated with the following September sea ice extent[Williams et al., 2016]. The AO drives dynamic thinning of the sea ice in the Eurasian Arctic during winter [Rigor et al., 2002] and influences the summer minimum. [Brunette et al., 2019] also showed that coastal divergence in winter correlates with the AO and influences September sea ice extent in the Laptev sea. Therefore, the underestimation of decadal variability in the CESM-LE in the Eurasian Arctic could be related to a weak representation of the two circulation regime in the Arctic described by Proshutinsky and Johnson (1997) or to small biases in the position of the Arctic High that leads to sea ice drift parallel to the coast as opposed to away from the coast [DeRepentigny et al., 2016]. It is important to note that the largest trend in sea ice loss over the last decades is observed in September in the East-Siberian sea [Onarheim et al., 2018] and only 10% of September sea ice loss in this region is explained by internal variability [England et al., 2019].

## 5.3 Pacific Sector

In the Pacific sector, the wavelet analysis has shown a location of important decadal variability just North of Bering strait. Bering strait is the only gate for Pacific waters to enter the Arctic Ocean. The Bering Strait inflow influences sea-ice by allowing oceanic heat to enter the broad Eurasian shelf and interact with sea ice [Woodgate et al., 2010]. It is important to note that sea ice decrease in the Bering sea is driven by both wind dynamics and thermodynamics [Frey et al., 2015]. Woodgate et al. (2012) showed that the Bering strait inflow has been increasing by 50% in the recent decades, leading a significant increase in heat transport [Woodgate et al., 2012]. The CESM-LE underestimates heat trans-

port through the Bering Strait [Auclair and Tremblay, 2018]. For the same time period, the storminess activity over the Arctic Ocean increased as well, augmenting heat exchange [Maslowski et al., 2000]. Pacific Decadal Oscillations (PDO) has a signature in the 15-to-25 years variability [Mantua and Hare, 2002] and can cause flushing events of older ice out of the Arctic Basin [Lindsay and Zhang, 2005]. The strength of the Aleutian Low and the Arctic High sets the sea surface height across the Bering Strait and therefore the volume flux across the strait. The wind in the Bering Strait reduces the magnitude of the volume flux trough the Bering strait. Therefore, variability in both the AO and the PDO can have a large influence on the Bering Strait OHT, on the Beafort Gyre and on the sea conditions in the Chukchi and East-Siberian sea. It has been shown that the PDO could be used to increase skill in decadal-scale predictability of the Arctic up to 7 years [Screen and Francis, 2016]. Our study show that this number can not be improved because climate model already show a weak but accurate decadal variability in this sector.

## 5.4 Future evolution

Inter-annual variability is increasing in every regions of the Arctic and is projected to continue to rise in the following decades [Jahn et al., 2016]. According to the CESM-LE, it should reach a maximum in 2030 and decrease due to the lack of sea ice afterwards. Year to year ice extent are less predictable in a transient climate between ice-covered and seasonally ice-free Arctic. Decadal variability (8-16 year period) is also expected to rise and reach a maximum in the future decades. The maximum happens slightly earlier in the Eurasian sector and slightly later in the Pacific sector due to difference in the remaining ice cover. Signs of increased decadal variability are visible in the observations, meaning that the rise in decadal variability happens later in CESM (10-20 years) than in the observations. Ocean

heat flux is a key factor in determining the ice edge positions, especially at high latitude [Bitz et al., 2005]. As Arctic sea ice continues to retreat following global warming, rapid September sea ice decline are expected to become increasingly correlated with variability in the atmosphere-ice heat fluxes [Auclair and Tremblay, 2018]. Analysis of the CESM-LE sea ice for 2020-2060 show that the spread in variability across ensemble members is increasing which might be due to the growing important of atmosphere-ice interaction. The spatial location of decadal variability varies, but the most common scenario is an increase of decadal variability in the Atlantic region, roughly following the path of the Transpolar drift stream. The exact location of the zone of high variability is slightly different across ensemble members. This could correspond to variation in the position of the Arctic high, giving further evidence for atmosphere-driven variability.

# 6

# Conclusion

We study long term variability in Arctic minimum sea ice extent where longer time series exist. More precisely, we study decadal variability in min SIE from the *Gridded Monthly Sea Ice Extent and Concentration, 1850 Onward, Version 1.1* and from the Community Earth system Model Large Ensemble using wavelet analysis. We show that sea ice extent decadal variability is underestimated in the CESM-LE in the Eurasian sector of the Arctic, more precisely in the East-Siberian sea, and overestimated in the Greenland sea. Decadal variability from the CESM-LE is in line with observations in the Pacific sector of the Arctic and in the Barents sea. Our current understanding of sea ice variability in the Eurasian sector of the Arctic allows us to presume that mechanisms of coastal divergence in the East-Siberian sea are not well represented in the CESM-LE, likely due to biases in the position of the climatologic Arctic High pressure system. Decadal variability of these atmospheric processes appear to be underestimated in the CESM-LE, and increasing this variability would also increase sea ice extent variability in the Eurasian sector of the Arctic leading to more uncertainties in prediction the evolution of sea ice.

In the Greenland sea, the slightly overestimated decadal variability that we have found is related to oceanic heat transport variations in Atlantic waters. We can link the observed variability to the AMOC and the BSO heat transport variability and to patterns of recirculation in the Greenland sea. The Atlantic sector of the Arctic is the only one where we can hope to decrease decadal variability in the CESM-LE.

Simulated min SIE decadal variability is in line with observations in the Pacific sector of the Arctic, where the Bering Ocean Heat Transport (OHT) has a larger impact on SIE decline. A Pacific-centric sea ice decline is expected in the Arcitc [DeRepentigny et al., 2016], which is in line with Bering OHT anomaly having a broader impact on min SIE because water enters on a broad shelf in Eurasia [Auclair and Tremblay, 2018]. Therefore, the simulated decline in SIE may be realistic in the Pacific sector of the Arctic, and in the whole Arctic given that the larger impacts of variability in this region. Since long term variability in the CESM is in line with observations, we do not expect to be able to decrease the uncertainty of the timing of an ice-free Arctic. The 21 years of uncertainty in the timing of an ice-free Arctic [Jahn et al., 2016] appear to be realistic or may even increase following a modified and more accurate representation of the atmospheric processes influencing sea ice in the East-Siberian sea, especially as they are expected to take a dominant place in triggering rapid sea ice decreases over shallow shelves [Auclair and Tremblay, 2018].

Finally, our study suggests the presence of a transition period between an ice-covered and seasonally ice-free Arctic characterised by increased variability at all time scales. We suggest that we are already in the transition period. Mechanisms of decadal variability that were understood for the last decades might not influence Arctic sea ice extent the same

way in a transient climate. Other climate indices than SIE need to be study to understand climate in the Arctic, as one number can not represent the whole Arctic and its complex dynamic. Regional studies focused on mechanisms specific for the regions might be key for understanding the changing response of the sea ice to atmospheric and oceanic processes.

# Bibliography

[Årthun et al., 2012] Årthun, M., Eldevik, T., Smedsrud, L. H., Skagseth, Ã., and Ingvaldsen, R. B. (2012). Quantifying the influence of atlantic heat on barents sea ice variability and retreat. *Journal of Climate*, 25(13):4736–4743.

[Årthun and Schrum, 2010] Årthun, M. and Schrum, C. (2010). Ocean surface heat flux variability in the barents sea. *Journal of Marine Systems*, 83(1):88 – 98.

[Aksenov et al., 2016] Aksenov, Y., Karcher, M., Proshutinsky, A., Gerdes, R., de Cuevas, B., Golubeva, E., Kauker, F., Nguyen, A. T., Platov, G. A., Wadley, M., Watanabe, E., Coward, A. C., and Nurser, A. J. G. (2016). Arctic pathways of pacific water: Arctic ocean model intercomparison experiments. *Journal of Geophysical Research: Oceans*, 121(1):27–59.

[Arctic and Antarctic Research Institute, 2007] Arctic and Antarctic Research Institute (2007). Sea ice charts of the russian arctic in gridded format, 1933-2006, version 1. compiled by v. smolyanitsky, v. borodachev, a. mahoney, f. fetterer, and r. g. barry. *Boulder, Colorado USA. NSIDC: National Snow and Ice Data Center*.

[Auclair and Tremblay, 2018] Auclair, G. and Tremblay, L. B. (2018). The role of ocean heat transport in rapid sea ice declines in the community earth system model large ensemble. *Journal of Geophysical Research: Oceans*, 123(12):8941–8957.

## BIBLIOGRAPHY

[Bitz et al., 2005] Bitz, C. M., Holland, M. M., Hunke, E. C., and Moritz, R. E. (2005). Maintenance of the sea-ice edge. *Journal of Climate*, 18(15):2903–2921.

[Bitz and Lipscomb, 1999] Bitz, C. M. and Lipscomb, W. H. (1999). An energy-conserving thermodynamic model of sea ice. *Journal of Geophysical Research: Oceans*, 104(C7):15669–15677.

[Blackman and Tukey, 1958a] Blackman, R. B. and Tukey, J. W. (1958a). The measurement of power spectra from the point of view of communications engineering âĂŤ part i. *Bell System Technical Journal*, 37(1):185–282.

[Blackman and Tukey, 1958b] Blackman, R. B. and Tukey, J. W. (1958b). The measurement of power spectra from the point of view of communications engineering âĂŤ part ii. *Bell System Technical Journal*, 37(2):485–569.

[Brunette et al., 2019] Brunette, C., Tremblay, B., and Newton, R. (2019). Winter coastal divergence as a predictor for the minimum sea ice extent in the laptev sea. *Journal of Climate*, 32(4):1063–1080.

[C. Hunke and Lipscomb, 2008] C. Hunke, E. and Lipscomb, W. (2008). CICE: The Los Alamos sea ice model documentation and software user's manual version 4.0 LA-CC-06-012. *Tech. Rep. LA-CC-06-012*.

[Cooley and Tukey, 1965] Cooley, J. and Tukey, J. (1965). An algorithm for the machine calculation of complex fourier series. *Mathematics of Computation*, 19(90):297–301.

[Danabasoglu et al., 2012] Danabasoglu, G., Bates, S. C., Briegleb, B. P., Jayne, S. R., Jochum, M., Large, W. G., Peacock, S., and Yeager, S. G. (2012). The CCSM4 ocean component. *Journal of Climate*, 25(5):1361–1389.

## BIBLIOGRAPHY

[Day et al., 2012] Day, J. J., Hargreaves, J. C., Annan, J. D., and Abe-Ouchi, A. (2012). Sources of multi-decadal variability in arctic sea ice extent. *Environmental Research Letters*, 7(3):034011.

[Delworth et al., 2013] Delworth, T. L., Zhang, R., and Mann, M. E. (2013). *Decadal to Centennial Variability of the Atlantic from Observations and Models*, pages 131–148. American Geophysical Union (AGU).

[DeRepentigny et al., 2016] DeRepentigny, P., Tremblay, L. B., Newton, R., and Pfirman, S. (2016). Patterns of sea ice retreat in the transition to a seasonally ice-free Arctic. *Journal of Climate*, 29(19):6993–7008.

[Dewdney, 1979] Dewdney, J. C. (1979). Chapter 2 - climate, soils, vegetation. In *A Geography of the Soviet Union (Third Edition)*, Pergamon Oxford Geographies, pages 17 – 37. Pergamon Press.

[England et al., 2019] England, M., Jahn, A., and Polvani, L. (2019). Nonuniform contribution of internal variability to recent arctic sea ice loss. *Journal of Climate*, 32(13):4039–4053.

[Frey et al., 2015] Frey, K. E., Moore, G., Cooper, L. W., and Grebmeier, J. M. (2015). Divergent patterns of recent sea ice cover across the bering, chukchi, and beaufort seas of the pacific arctic region. *Progress in Oceanography*, 136:32 – 49. Synthesis of Arctic Research (SOAR).

[Frolov et al., 2009] Frolov, I., Gudkovichand, Z., Karlin, V., G., K. E., and Smolyanitsky, V. (2009). *Climate Change in Eurasian Arctic Shelf Seas*. Journal of Geophysical Research: Oceans.

## BIBLIOGRAPHY

[Gent et al., 2011] Gent, P. R., Danabasoglu, G., Donner, L. J., Holland, M. M., Hunke, E. C., Jayne, S. R., Lawrence, D. M., Neale, R. B., Rasch, P. J., Vertenstein, M., Worley, P. H., Yang, Z.-L., and Zhang, M. (2011). The community climate system model version 4. *Journal of Climate*, 24(19):4973–4991.

[Gilman et al., 1963] Gilman, D. L., Fuglister, F. J., and Mitchell, J. M. (1963). On the power spectrum of red noise. *Journal of the Atmospheric Sciences*, 20(2):182–184.

[Holland et al., 2006] Holland, M. M., Bitz, C. M., and Tremblay, B. (2006). Future abrupt reductions in the summer arctic sea ice. *Geophysical Research Letters*, 33(23).

[Hunke and Dukowicz, 2002] Hunke, E. C. and Dukowicz, J. K. (2002). The elastic-viscous-plastic sea ice dynamics model in general orthogonal curvilinear coordinates on a sphere-incorporation of metric terms. *Monthly Weather Review*, 130(7):1848–1865.

[Hurrell et al., 2003] Hurrell, J. W., Kushnir, Y., Ottersen, G., and Visbeck, M. (2003). *An Overview of the North Atlantic Oscillation*, pages 1–35. American Geophysical Union (AGU).

[Itkin and Krumpen, 2017] Itkin, P. and Krumpen, T. (2017). Winter sea ice export from the laptev sea preconditions the local summer sea ice cover and fast ice decay. *The Cryosphere*, 11(5):2383–2391.

[Jahn et al., 2016] Jahn, A., Kay, J. E., Holland, M. M., and Hall, D. M. (2016). How predictable is the timing of a summer ice-free Arctic? *Geophysical Research Letters*, 43(17):9113–9120.

[Kay et al., 2015] Kay, J. E., Deser, C., Phillips, A., Mai, A., Hannay, C., Strand, G., Arblaster, J. M., Bates, S. C., Danabasoglu, G., Edwards, J., Holland, M., Kushner, P.,

Lamarque, J.-F., Lawrence, D., Lindsay, K., Middleton, A., Munoz, E., Neale, R., Oleson, K., Polvani, L., and Vertenstein, M. (2015). The Community Earth System Model (CESM) large ensemble project: A community resource for studying climate change in the presence of internal climate variability. *Bulletin of the American Meteorological Society*, 96(8):1333–1349.

[Kelly, 1979] Kelly, P. M. (1979). An Arctic sea ice data set, 1901-1956. *Glaciological Data*, Report GD-5: Workshop on Snow Cover and Sea Ice Data:National Snow and Ice Data Center: 101–110.

[Kim et al., 2018] Kim, W. M., Yeager, S., Chang, P., and Danabasoglu, G. (2018). Low-frequency north atlantic climate variability in the community earth system model large ensemble. *Journal of Climate*, 31(2):787–813.

[Kwok et al., 2013] Kwok, R., Spreen, G., and Pang, S. (2013). Arctic sea ice circulation and drift speed: Decadal trends and ocean currents. *Journal of Geophysical Research: Oceans*, 118(5):2408–2425.

[Lawrence et al., 2011] Lawrence, D. M., Oleson, K. W., Flanner, M. G., Thornton, P. E., Swenson, S. C., Lawrence, P. J., Zeng, X., Yang, Z.-L., Levis, S., Sakaguchi, K., Bonan, G. B., and Slater, A. G. (2011). Parameterization improvements and functional and structural advances in version 4 of the community land model. *Journal of Advances in Modeling Earth Systems*, 3(1).

[Lesgaft, 1913] Lesgaft, E. (1913). *Arctic Ocean Ice and a Seaway from Europe to Siberia*. St. Petersburg. [in Russian].

## BIBLIOGRAPHY

[Lindsay and Zhang, 2005] Lindsay, R. W. and Zhang, J. (2005). The thinning of arctic sea ice, 1988-2003: Have we passed a tipping point? *Journal of Climate*, 18(22):4879–4894.

[M. Holland et al., 2008] M. Holland, M., Bitz, C., Tremblay, B., and Bailey, D. (2008). The role of natural versus forced change in future rapid summer Arctic ice loss. *Washington DC American Geophysical Union Geophysical Monograph Series*, 180.

[Mantua and Hare, 2002] Mantua, N. J. and Hare, S. R. (2002). The pacific decadal oscillation. *Journal of Oceanography*, 58(1):35–44.

[Maslowski et al., 2000] Maslowski, W., Newton, R., Schlosser, P., J. Semtner, A., and Martinson, D. (2000). Modeling recent climate variability in the arctic ocean. *Geophysical Research Letters - GEOPHYS RES LETT*, 27.

[Meehl et al., 2013] Meehl, G. A., Washington, W. M., Arblaster, J. M., Hu, A., Teng, H., Kay, J. E., Gettelman, A., Lawrence, D. M., Sanderson, B. M., and Strand, W. G. (2013). Climate change projections in CESM1(CAM5) compared to CCSM4. *Journal of Climate*, 26(17):6287–6308.

[Meier et al., 2013] Meier, W. N., Fetterer, F., Savoie, M., Mallory, S., Duerr, R., and Stroeve, J. (2013). NOAA/NSIDC climate data record of passive microwave sea ice concentration, version 2. *Boulder, Colorado USA. NSIDC: National Snow and Ice Data Center*.

[Meinshausen et al., 2011] Meinshausen, M., Smith, S. J., Calvin, K., Daniel, J. S., Kainuma, M. L. T., Lamarque, J.-F., Matsumoto, K., Montzka, S. A., Raper, S. C. B., Riahi, K., Thomson, A., Velders, G. J. M., and van Vuuren, D. P. (2011). The RCP green-

house gas concentrations and their extensions from 1765 to 2300. *Climatic Change*, 109(1):213.

[Melia et al., 2016] Melia, N., Haines, K., and Hawkins, E. (2016). Sea ice decline and 21st century trans-arctic shipping routes. *Geophysical Research Letters*, 43(18):9720–9728.

[Mercier et al., 2015] Mercier, H., Lherminier, P., Sarafanov, A., Gaillard, F., Daniault, N., Desbruyères, D., Falina, A., Ferron, B., Gourcuff, C., Huck, T., and Thierry, V. (2015). Variability of the meridional overturning circulation at the Greenland –Portugal OVIDE section from 1993 to 2010. *Progress in Oceanography*, 132:250 – 261. Oceanography of the Arctic and North Atlantic Basins.

[Muilwijk et al., 2018] Muilwijk, M., Smedsrud, L. H., Ilicak, M., and Drange, H. (2018). Atlantic water heat transport variability in the 20th century arctic ocean from a global ocean model and observations. *Journal of Geophysical Research: Oceans*, 123(11):8159–8179.

[Nansen, 1915] Nansen, F. (1915). *To the Country of the Future*. Petrograd. [in Russian].

[Notz and Stroeve, 2018] Notz, D. and Stroeve, J. (2018). The trajectory towards a seasonally ice-free Arctic ocean. *Current Climate Change Reports*, 4(4):407–416.

[Onarheim et al., 2018] Onarheim, I. H., Eldevik, T., Smedsrud, L. H., and Stroeve, J. C. (2018). Seasonal and regional manifestation of Arctic sea ice loss. *Journal of Climate*, 31(12):4917–4932.

## BIBLIOGRAPHY

[Orvik and Skagseth, 2003] Orvik, K. A. and Skagseth, Ã. (2003). The impact of the wind stress curl in the north atlantic on the atlantic inflow to the norwegian sea toward the arctic. *Geophysical Research Letters*, 30(17).

[Peng et al., 2013] Peng, G., Meier, W. N., Scott, D. J., and Savoie, M. H. (2013). A long-term and reproducible passive microwave sea ice concentration data record for climate studies and monitoring. *Earth System Science Data*, 5(2):311–318.

[Press et al., 2007] Press, W. H., Teukolsky, S. A., Vetterling, W. T., and Flannery, B. P. (2007). *Numerical Recipes 3rd Edition: The Art of Scientific Computing*. Cambridge University Press, New York, NY, USA, 3 edition.

[Proshutinsky et al., 2015] Proshutinsky, A., Dukhovskoy, D., Timmermans, M.-L., Krishfield, R., and Bamber, J. L. (2015). Arctic circulation regimes. *Philosophical Transactions of the Royal Society A: Mathematical, Physical and Engineering Sciences*, 373(2052):20140160.

[Proshutinsky and Johnson, 1997] Proshutinsky, A. Y. and Johnson, M. A. (1997). Two circulation regimes of the wind-driven Arctic ocean. *Journal of Geophysical Research: Oceans*, 102(C6):12493–12514.

[Rigor et al., 2002] Rigor, I. G., Wallace, J. M., and Colony, R. L. (2002). Response of sea ice to the arctic oscillation. *Journal of Climate*, 15(18):2648–2663.

[Screen and Francis, 2016] Screen, J. and Francis, J. (2016). Contribution of sea-ice loss to arctic amplification is regulated by pacific ocean decadal variability. *Nature Climate Change*, 6.

## BIBLIOGRAPHY

[Screen and Deser, 2019] Screen, J. A. and Deser, C. (2019). Pacific ocean variability influences the time of emergence of a seasonally ice-free arctic ocean. *Geophysical Research Letters*, 46(4):2222–2231.

[Simpkins, 2018] Simpkins, G. (2018). Arctic storms. *Nature Climate Change*, 8.

[Torrence and Compo, 1998] Torrence, C. and Compo, G. P. (1998). A practical guide to wavelet analysis. *Bulletin of the American Meteorological Society*, 79(1):61–78.

[Vize, 1940] Vize, V. Y. (1940). Climate of the Soviet Arctic Seas. Moscow: Glavsevmorput [in Russian].

[Vize, 1944] Vize, V. Y. (1944). Hydrological conditions in the ice edge area in the Arctic seas. AARI Proc., 184, 125-151 [in Russian].

[Walsh and M. Johnson, 1979] Walsh, J. and M. Johnson, C. (1979). An analysis of Arctic sea ice fluctuations, 1953-77. *Journal of Physical Oceanography*, 9:580–591.

[Walsh, 1978] Walsh, J. E. (1978). A data set on northern hemisphere sea ice extent. *Glaciological Data*, Report GD-2, part 1:National Snow and Ice Data Center: 49–51.

[Walsh et al., 2016a] Walsh, J. E., Chapman, W. L., and Fetterer, F. (2015, updated 2016a). Gridded monthly sea ice extent and concentration, 1850 onward, version 1.1. *Boulder, Colorado USA. NSIDC: National Snow and Ice Data Center*.

[Walsh et al., 2016b] Walsh, J. E., Fetterer, F., Scott Stewart, J., and Chapman, W. L. (2016b). A database for depicting Arctic sea ice variations back to 1850. *Geographical Review*, 107(1):89–107.

[Wang et al., 2009] Wang, J., Zhang, J., Watanabe, E., Ikeda, M., Mizobata, K., Walsh, J. E., Bai, X., and Wu, B. (2009). Is the dipole anomaly a major driver to record lows in arctic summer sea ice extent? *Geophysical Research Letters*, 36(5).

[Williams et al., 2016] Williams, J., Tremblay, B., Newton, R., and Allard, R. (2016). Dynamic preconditioning of the minimum september sea-ice extent. *Journal of Climate*, 29(16):5879–5891.

[Woodgate et al., 2010] Woodgate, R. A., Weingartner, T., and Lindsay, R. (2010). The 2007 bering strait oceanic heat flux and anomalous Arctic sea-ice retreat. *Geophysical Research Letters*, 37(1).

[Woodgate et al., 2012] Woodgate, R. A., Weingartner, T. J., and Lindsay, R. (2012). Observed increases in bering strait oceanic fluxes from the pacific to the arctic from 2001 to 2011 and their impacts on the arctic ocean water column. *Geophysical Research Letters*, 39(24).

[Wu et al., 2006] Wu, B., Wang, J., and Walsh, J. E. (2006). Dipole anomaly in the winter arctic atmosphere and its association with sea ice motion. *Journal of Climate*, 19(2):210–225.

[Yan et al., 2018] Yan, X., Zhang, R., and Knutson, T. R. (2018). Underestimated amoc variability and implications for amv and predictability in cmip models. *Geophysical Research Letters*, 45(9):4319–4328.

[Zhang et al., 2018] Zhang, J., Stegall, S. T., and Zhang, X. (2018). Wind–sea surface temperature–sea ice relationship in the Chukchi–Beaufort seas during autumn. *Environmental Research Letters*, 13(3):034008.

## BIBLIOGRAPHY

[Zhang et al., 2019] Zhang, R., Sutton, R., Danabasoglu, G., Kwon, Y.-O., Marsh, R., Yeager, S. G., Amrhein, D. E., and Little, C. M. (2019). A review of the role of the atlantic meridional overturning circulation in atlantic multidecadal variability and associated climate impacts. *Reviews of Geophysics*, 0(0).

# 7

# Appendix

## 7.1 Fourier Analysis

Before using wavelet analysis, we used Fourier analysis to get preliminary results and understand the problem. This section briefly describes this method and our findings.

### 7.1.1 Method

We first use a discrete Fourier transform (DFT) to study the variability of the sea ice. DFT allows the representation of a signal in the frequency domain, frequencies being associated to sine and cosine modes. The DFT is defined as:

$$H_n = \sum_{k=0}^{N-1} h_k e^{2\pi i k n/N}, \tag{7.1}$$

where $H_n$ is the Fourier coefficients and $h_k$ being the points of the time series [Press et al., 2007]. The fast Fourier transform (FFT) is the algorithm that we use to com-

pute the DFT [Cooley and Tukey, 1965, Press et al., 2007]. A decadal variability would correspond to a peak at a period approximately 10 years while multi-decadal variability would be associated with a respond at smaller frequencies. We use the FFT algorithm on sea ice extent anomalies (i.e. deviation from the ensemble mean for CESM-LE and linear detrending on observations). The anomalies are in percentage of the area of the sea, so that we can compare the different peripheral seas altogether and with the whole Arctic ocean. We also use a Hann window before computing the FFT to reduce the edge effects [Blackman and Tukey, 1958a, Blackman and Tukey, 1958b].

### 7.1.2 Results and discussion

Looking at the September sea ice extent in the entire Arctic ocean, we see almost steady conditions for observations and model outputs until 1990, where we start to observe a rapid decline (see figure 7.1, top). The interannual variability increases before reducing again in models around 2050, due to ice-free conditions in most of the ensemble members. The instability of the climate allows us to expect a change of regime in these periods. Computing the DFT as explained in the previous section shows multi-decadal variability for both CESM-LE ensemble mean and SIBT1850 (see figure 7.1, bottom). We see a relatively big tail at high frequencies and a peak at frequency 1.25 for the SIBT1850. This peak means that a sine wave associated with a period of 8 years with an amplitude of 0.7% of the total area of the sea is an important component of the initial signal. We can produce two spectrum, one for before 1990 and one for after 1990, but the time resolution would be reduced over the point of usefulness. A wavelet spectrum would be more appropriate for this kind of analysis.

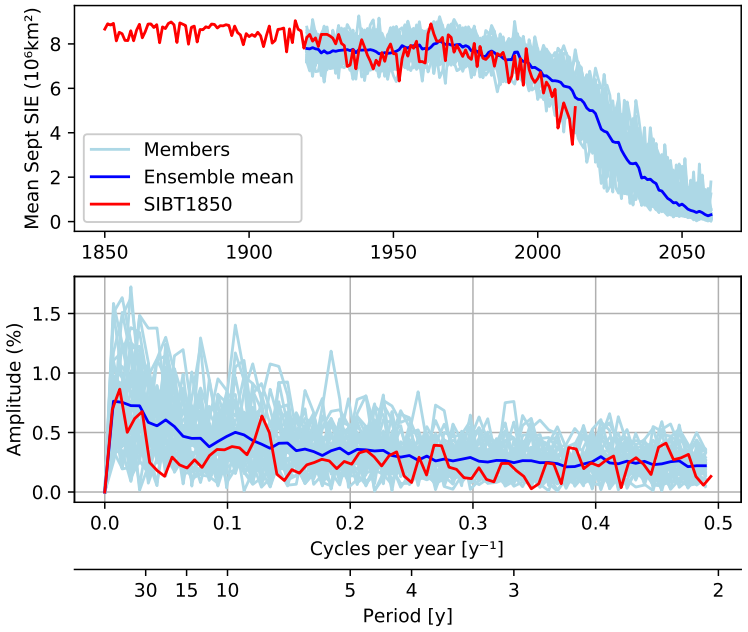


Figure 7.1: September sea ice extent in $10^6$ $km^2$ (top figure) and Fourier transform of September sea ice anomaly in percentage of the area of the sea (bottom figure) for the whole Arctic Ocean

We study the September sea ice variability in the peripheral seas of the Arctic (figure 7.1). The Barents sea shows some multi-decadal variability, but no mode in particular is really dominant. A tail in the high frequencies is present, and this is the case for all peripheral seas, ranging from 0.5 to 2% of the area for every frequency. The ensemble mean of the CESM-LE has a bigger amplitude than SIBT1850 and it's variability is generally larger. That can be because of the abrupt sea ice decrease that we face after 1990. We notice that the sea ice extent in SIBT1850 is generally much smaller than the ensemble mean of the CESM-LE for the whole period where they coincide, and it's interannual variability is quite small. That would also explain the difference in amplitude from the bottom figure.

The DFT of September sea ice anomaly from Kara sea shows a 5% peak at a period

of 160 years and almost no decadal and multi-decadal variability from the SIBT1850. The CESM-LE doesn't show any interesting result.

In the Laptev sea, the observations and the model seem to show a similar sea ice extent. The interannual variability is big, sometimes ranging from almost ice-free to full of ice in two years. The Fourier spectrum are similar, with some variability in the 5-10 years range for SIBT1850.

Like it was the case in the Laptev sea, the East-Siberian September sea ice extent varies a lot over the time series, from almost fully covered to ice-free. The spectrum from SIBT1850 and CESM-LE are similar.

The representation of the ice extent in the Chukchi sea is quite good up to 1850 in SIBT1850 thanks to American whaling ship records. The ensemble mean of CESM-LE doesn't show any particular mode of variability, but the SIBT1850 clearly shows multi-decadal variability and a approximately 8 years cycle. High frequencies are also quite important. The Chukchi sea is an important point of convergence (and divergence) for Pacific waters going in the Arctic ocean from the Bering strait [Aksenov et al., 2016]. It could be a signature of Pacific Decadal Oscillations.

We can see the same multidecadal and 8 years variability in the DFT of Beaufort's September sea ice anomaly from SIBT1850. The amplitude is smaller but the peaks are still there. That would be consistent since some of the currents in the Beaufort sea come from Chukchi sea and Bering strait [Aksenov et al., 2016]. The sea ice extent is big in the observations compared to models, but spectrum show bigger amplitude for CESM-LE.

The spectrum from sea ice extent anomaly in Greenland sea shows a significant tail in the high frequency and not much decadal climate variability. The model seems to slightly

overestimate the variability compared to observations.

We split the Arctic in two regions according to the regions of F2009, which is Greenland, Barents ans Kara sea (GBK) and Laptev, East-Siberian and Chukchi seas (LEC). We obtain an additional spectra from sea ice extent observations in August using F2009 sea ice extent (see figure 7.2). In the region GBK, we observe some multidecadal variability in the observations (both F200 and SIBT1850) and not much in the model. The observations and the model seem to agree in their amplitude. For the region LEC, there is a strong 8 years cycle in F2009 but also in SIBT1850. Multidecadal oscillations are present in both the observations and the model. In general, we can conclude that SIBT1850 and F2009 are in agreement with one another (relative to their sea ice extent and variability).

## 7.1 Fourier Analysis

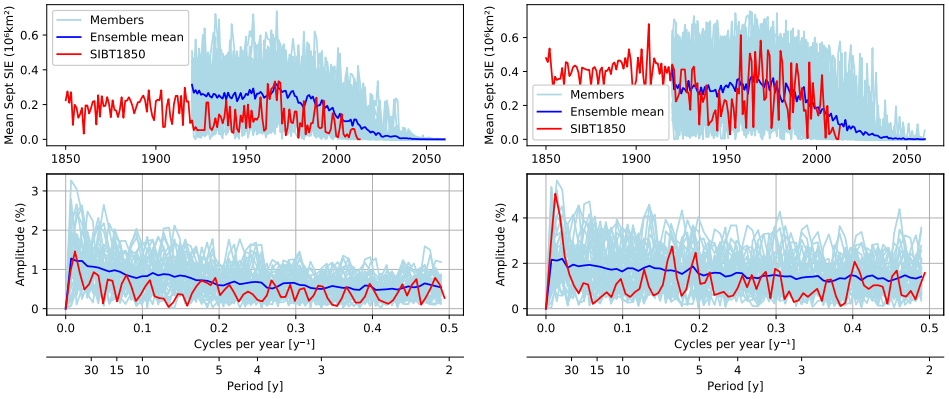


(a)




(b)

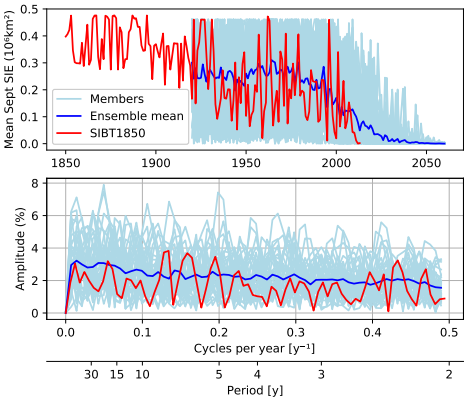


(c)

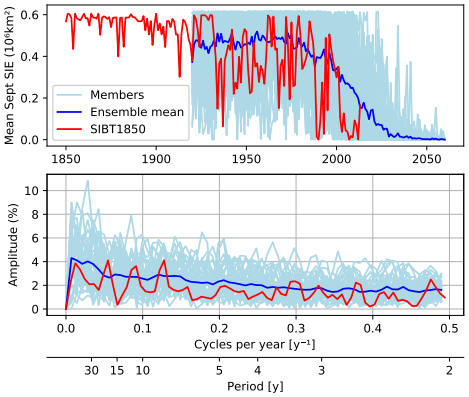


(d)

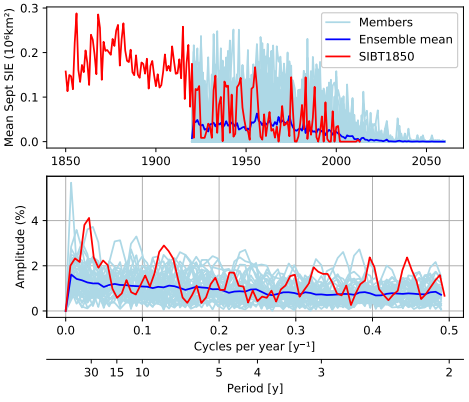


(e)

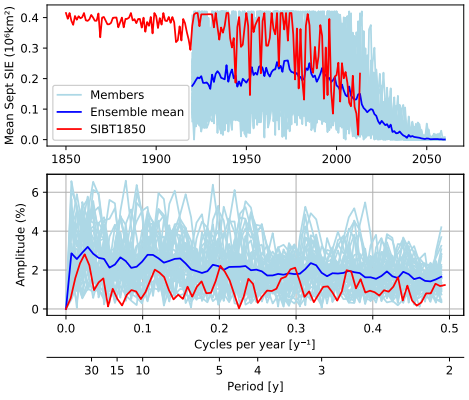


(f)

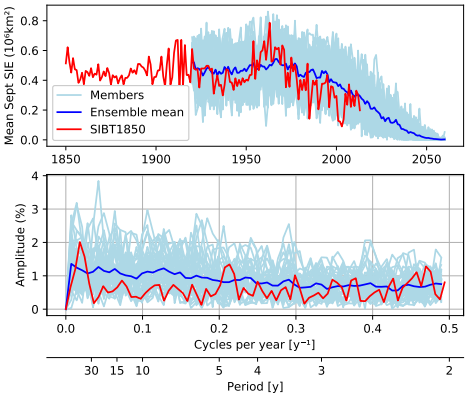


(g)

Figure 7.1: September sea ice extent in $10^6$ km$^2$ (top figure) and Fourier transform of September sea ice anomaly in percentage of the area of the sea (bottom figure) for a) Barents Sea, b) Kara Sea, c) Laptev Sea, d) East-Siberian Sea, e) Chukchi Sea, f) Beaufort Seas and g) Greenland Sea. The ensemble mean of the CESM-LE is in dark blue while individual ensemble members are in light blue and the SIBT1850 is in red.

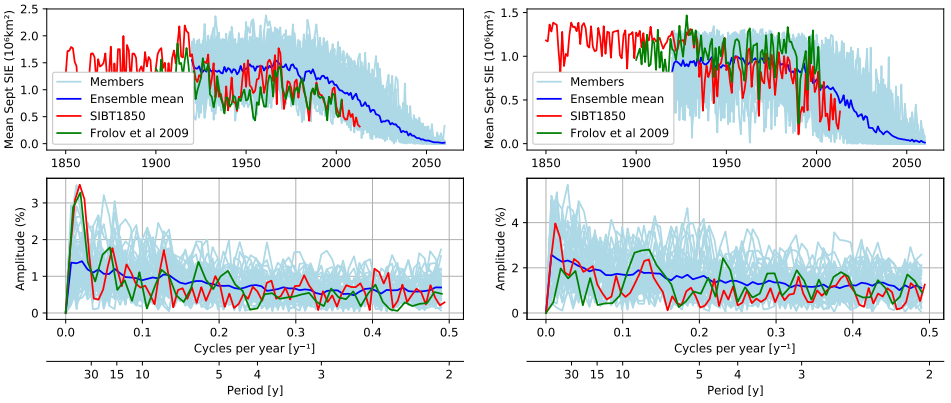


(a) (b)

Figure 7.2: August sea ice extent in $10^6$ km$^2$ (top figure) and Fourier transform of August sea ice anomaly in percentage of the area of the sea (bottom figure) for a) Greenland, Barents and Kara Seas, b) Laptev, East-Siberian and Chukchi Seas. The ensemble mean of the CESM-LE is in dark blue while individual ensemble members are in light blue, the SIBT1850 is in red and F2009 is in green.